# STRUCTURAL AND MICROSTRUCTURAL PROPERTIES OF IN-SITU ALUMINA-TITANIA-GRAPHITE HYBRID NANOCOMPOSITE VIA LOW ENERGY MILLING

by

**NURUL ADILLAH FARHANA AB MALEK**

A report submitted in fulfilment of the requirement for the degree of Bachelor of Applied Science (Materials Technology)

**FACULTY OF EARTH SCIENCE**
**UNIVERSITI MALAYSIA KELANTAN**
**2016**

## DECLARATION

I declare that this thesis entitled "STRUCTURAL AND MICROSTRUCTURAL PROPERTIES OF IN-SITU ALUMINA-TITANIA-GRAPHITE HYBRID NANOCOMPOSITE VIA LOW ENERGY MILLING" is the result of my own research except as cited in the references. The thesis has not been accepted for any degree and is not concurrently submitted in candidature of any other degree.

Signature : _____

Name : Nurul Adillah Farhana binti Abdul Malek

Date : 4 January 2017

## ACKNOWLEDGEMENT

I would like to acknowledge the authority of Faculty of Earth Science, Universiti Malaysia Kelantan for giving me an opportunity to do my research for the final year project. Also, I would like to express my gratitude to a number of people who had been supporting me in the achievement of this final year project.

First of all, thank you so much to my supervisor, Dr Mahani Yusoff for providing me guidelines and advices in the completion of this research project. I would also like to thank the Dean of Faculty of Earth Science, Prof Ibrahim Busu and also lab assistance, Encik Firdaus for supporting and help me throughout the research project. In addition, thank you to all the lecturers and staff who had helped me directly and indirectly throughout the completion of this final year project. A special thanks to my beloved mother, Norhayati Shabidin, my sister Nurul Liyana Amanina and my partner, Abdul Hazwan for being supportive in all matters. Also, thanks to my friends and especially my roommate Ain, and family who had helped me in completing this research project. Last but not least, thanks to final year project team (Syuhada, Nazihah, Asma, Huda, Alya and Farihah) that stayed together as a team throughout the final year project. Thank you.

**STRUCTURAL AND MICROSTRUCTURAL PROPERTIES OF IN-SITU ALUMINA-TITANIA-GRAPHITE HYBRID NANOCOMPOSITE VIA LOW ENERGY MILLING**

## ABSTRACT

This study was conducted to investigate the effect of variation milling time and compaction pressure on structural and microstructural of in situ $Al_2O_3$–$TiO_2$-graphite nanocomposite using powder metallurgy route. Elemental powders of $Al_2O_3$ (alumina) $TiO_2$ (titania) and graphite (C) were milled in a low energy mill using 10 mm alumina ball at 15, 30, 45 and 60 hours of milling. Then, the nanocomposite was compacted using cold compaction with 200 to 800 MPa. No new phase formed because the energy was not enough to initiate solid state reaction during milling. Diffusion of graphite into $Al_2O_3$ matrix was only obtained after 60 h of milling. The morphology of $Al_2O_3$–$TiO_2$-graphite powder become homogenous with increasing milling time while $Al_2O_3$ crystallite size was reduced and internal strain was increased. The densification of $Al_2O_3$–$TiO_2$-graphite nanocomposite was enhanced with increasing milling time and compaction pressure.

**SIFAT STRUKTUR DAN MIKROSTRUKTUR KOMPOSIT NANO HIBRID IN SITU ALUMINA-TITANIA-GRAFIT MELALUI PENGISARAN BERTENAGA RENDAH**

## ABSTRAK

Kajian ini dijalankan untuk mengkaji kesan variasi masa pengisaran dan tekanan pemadatan ke atas struktur dan mikrostruktur in situ $Al_2O_3$-$TiO_2$-grafit komposit nano menggunakan kaedah metalurgi serbuk. Serbuk alumina ($Al_2O_3$) titania ($TiO_{2)}$ dan grafit (C) telah dikisar menggunakan pengisar tenaga rendah dengan 10 mm bebola $Al_2O_3$ pada 15, 30, 45 dan 60 j pengisaran. Kemudian, komposit nano tersebut dipadatkan menggunakan pemadatan sejuk dengan 200-800 MPa. Tiada fasa baru terbentuk kerana tenaga yang tidak mencukupi untuk memulakan tindak balas keadaan pepejal semasa pengisaran. Penyerapan grafit ke dalam $Al_2O_3$ matriks hanya diperolehi selepas 60 h pengisaran. Morfologi serbuk $Al_2O_3$-$TiO_2$-grafit komposit nano menjadi sekata dengan peningkatan masa pengisaran manakala saiz hablur $Al_2O_3$ berkurang dan peningkatan terikan dalaman meningkat. Penumpatan $Al_2O_3$-$TiO_2$-grafit komposit nano meningkat dengan peningkatan masa pengisaran dan tekanan pemadatan.

## LIST OF TABLE

## TABLE OF CONTENTS

## LIST OF FIGURES

## LIST OF ABBEREVATIONS

| | |
|---|---|
| AD | Apparent Density |
| $Al_2O_3$ | Alumina |
| CMC | Ceramic Matrix Composite |
| COV | Coefficient of Variation |
| CVI | Chemical Vapour Infiltration |
| FTIR | Infrared Spectroscopy |
| GD | Green Density |
| MI | Melt Infiltration |
| MMC | Metal Matrix Composite |
| OM | Optical Microscopy |
| PE | Polyethylene |
| PIP | Polymer Impregnation Process |
| PM | Powder Metallurgy |
| PMC | Plastic Matrix Composite |
| PP | Polypropylene |
| SP | Sol Gel |
| TF | Theoritical Density |
| $TiO_2$ | Titania |
| UTS | Ultimate Tensile Strength |
| WH | Williamson Hall (WH) method |
| XRD | X-ray Diffraction |
| YS | Yield Stress |

## LIST OF SYMBOLS

| | |
|---|---|
| Å | Angstrom |
| $B_{cryst}$ | Broadening due to crystallite size |
| $B_i$ | Instrumental broadening |
| $B_o$ | Sum of the total broadening of size, lattice strain and instrument |
| $B_r$ | overall broadening |
| $B_{strain}$ | Broadening due to strain |
| cm | Centimetre |
| cps | Count per second |
| g | Gram |
| GPa | Giga Pascal |
| h | Hours |
| k | Constant |
| m | Mass |
| mm | Millimetre |
| MPa | Mega Pascal |
| nm | Nano metre |
| $^o$ | Degree |
| $^oC$ | Temperature |
| rpm | Rotate per minute |
| *V* | Volume |
| wt% | Weight percent |
| $\lambda$ | Wavelength |
| % | Percentage |
| µm | Micrometre |

# CHAPTER 1

# INTRODUCTION

## 1.1 Background of study

Ceramic matrix composites (CMC) exhibit superior properties due to combination of ceramic characteristics such as high strength, hardness and temperature stability with specific tailored properties (Aigbodion *et al.*, 2010; Low, 2014). CMC exhibit relatively high strength and stability, low density and chemical inertness. However, they are brittle, and are susceptible to thermal shock (Donald & McMillan, 1976). In order to overcome this problem, the fabrication process and development of ceramic nanocomposite has been investigated (Niihara *et al.*, 1993; Ohji *et al.*, 1998; Sternitzke, 1997). The matrices that commonly used are alumina ($Al_2O_3$), silicon carbide, magnesium oxide, silicon nitride and zirconium oxide. Among them, $Al_2O_3$ is the most common matrix because it has chemical and thermal stability, relatively good strength, thermal and electrical insulation characteristic and has abundance source (Auerkari, 1996).

Ceramic-based nanocomposite can be classified in two fundamental groups. One is composed of micrometer sized matrices dispersed with a nanometer second phase and another group is nanophase ceramic composites is nanocrystalline matrix composites, also called nanoceramics, in which the matrix grain size is below 100 nm. The nano–nano type microstructure will be formed when the second phase is also nano-scaled (Yongli, 2006). CMCs can also contain more than one type of reinforcements which known as hybrid nanocomposite.

$Al_2O_3$–$TiO_2$ composite has been widely used in machinery, textile and printing industry due to their high hardness, excellent wear, corrosion, chemical and thermal resistance. It also have been reported to possess superior toughness, adhesion, wear and corrosion resistance (Bian *et al.,* 2012). $Al_2O_3$ also can be reinforced using nanoparticles $TiO_2$ since nanostructured materials offers unique mechanical, optical, electrical and thermal properties. $Al_2O_3$–$TiO_2$ nanocomposite can be added with graphite to produce hybrid nanocomposite. Graphite can act as a lubricant since having a crystal structure with strongly linked atoms.

There are many methods used to fabricate $Al_2O_3$–$TiO_2$ composite such as rotating cube, precise casting, forging and powder metallurgy (Taghian *et al.*,2014). Powder Metallurgy (PM) is an alternative technique for composite fabrication. PM consists of three routes; mixing powder elements, compacting, and sintering. The advantage of PM compared to above techniques are PM produced powder with uniform chemical composition with desired characteristic, resulting from the absence of segregation during solidification. Furthermore, PM able to produce unique compositions including non-equilibrium compositions and microstructures such as crystalline, non-crystalline and amorphous. Besides, PM also can produce wide variety of materials, material with controlled porosity and materials with improved magnetic properties (Pournaderi *et al.,* 2012; Angelo *et al.,* 2012).

In more advanced processing, PM can be combined with in situ processing. In situ processing involves of internally mix matrix and reinforced material during the composite fabrication. In in-situ processing combine with PM provide good dispersion between matrix and reinforcement.

## 1.2 Problem Statement

$Al_2O_3$–$TiO_2$ nanocomposite is widely known having high hardness, high corrosion resistance, chemical and thermal resistance and high wear and corrosion resistance. However, $Al_2O_3$–$TiO_2$ composite has low toughness and ductility as well as not stable at high temperature. In order to overcome these problems, $Al_2O_3$–$TiO_2$ can be reinforced with graphite. Graphite is the most suitable material to be reinforced in $Al_2O_3$–$TiO_2$ to produce hybrid nanocomposite due to its ability to improve thermal stability, wear resistance and brittleness at the optimize composition.

## 1.3 Objective

The objectives of this research are:

1. To investigate the effect of milling time on structural and microstructural of in situ $Al_2O_3$–$TiO_2$-graphite nanocomposite.
2. To determine the variation of compaction pressure on densification of $Al_2O_3$–$TiO_2$-graphite composites.

## 1.4 Expected Outcome

It is expected that $Al_2O_3$–$TiO_2$-graphite nanocomposite enhance toughness and ductility of the $Al_2O_3$–$TiO_2$ composite so that it can be used in high performance application. The microstructure will have homogenous distribution of composite particles from combination between in situ processing and powder metallurgy.

# CHAPTER 2

# LITERATURE REVIEW

## 2.1 Composite

Composite can be defined as a combination of matrix and reinforcement, which when combined gives properties superior to the properties of the individual components. Composite materials can be classified into three categories which are metal matrix composites (MMC), polymer matrix composites (PMC) and ceramic matrix composites (CMC) (Banga *et al.*, 2015). The difference between these composites are different matrix materials and reinforced with nanoparticles.

MMCs are composed of metallic matrix that consist of ceramic or polymers reinforcements. The most common matrix use in metal matrix are aluminium, magnesium, titanium and copper (Casati *et al.*, 2014). They have been widely used in aerospace application, automobile engine parts, sports equipment and shipping industry (Vijayaraghavan, 2007). MMC possesses excellent properties which are high modulus, high strength, high wear resistance and ease of manufacturing (Prabu *et al* ., 2016). PMC are composed of matrix from thermoset (unsaturated polyester, epoxy) or thermoplastic (nylon, polystyrene) and embedded glass carbon, steel or Kevlar fibres (dispersed phase) (Banga *et al.*, 2015). Thermoplastics such as polypropylene (PP) and polyethylene (PE) are widely used (Bhattacharya *et al.*, 2007). PMC are mainly used in aerospace application due to their low cost and simple fabrication methods (Vijayaraghavan, 2007).

Meanwhile, CMC consist of ceramic as matrix and the reinforcements can be metals, ceramics or polymers. The most common matrices are $Al_2O_3$ and silicon nitride (Yongli, 2006). CMC are mostly used in high temperature application such as turbine and jet engines (Aigbodion *et al.*, 2010). The focus of this study is on ceramic based

composite, therefore the description on this type of composite will be further discuss in the next section.

### 2.1.1 Nanocomposite

Nanocomposites are the composites that one of the phases have at least indicates dimensions in the nanometer range (Yoon *et al.,* 2015). Nanocomposite substances have revealed suitable alternatives to overcome limitations of micro composite and monolithic, while posing preparation challenges related to the control of elemental composition and stoichiometry in the nanocluster phase. They have been used for improved physical properties, such as mechanical, thermal, water resistance, gas barrier properties and electrical properties (Yoon *et al.,* 2015).

Nanocomposites may consist at least one or more phases with nanoscale dimensions (0-D, 1- D, and 2-D) that embedded in metal, ceramic, or polymer matrices. Nanocomposite exhibits superior mechanical and physical properties compared to their respective matrix materials (Çelik *et al.,* 2016). Ceramic matrix can be reinforced with nanomaterial to become nanocomposite. The mechanical properties of ceramics are known improved significantly by dispersion of nanometer-sized ceramic particles into the ceramic-matrix grains or grain boundaries. The advantage of ceramic nanocomposite lies not only in strength but also in other mechanical properties such as fracture toughness, hardness, and creep resistance (Ohji *et al.,* 1998). Nano phase ceramic composites is nanocrystalline matrix composites, also called Nano ceramics, in which the matrix grain size is below 100 nm. Nano ceramics exhibit promising properties due to the changes in deformation mechanisms when the grain size is reduced to 100 nm (Yongli, 2006).

.

### 2.1.1 Hybrid nanocomposite

The general definition of hybrids is composite structures containing at least two types of reinforcements (Wagner *et al.,* 1982). Yamada, 1989 defined hybrid materials as mixtures of two or more materials with new properties created by new electron orbitals formed between each material. While Makisima, 2004 defines hybrid nanocomposite is sub-micron level mixture of similar kinds of materials. In the other hand, hybrid nanocomposite is a material created by dispersing inorganic nanoparticulates into a macroscopic organic matrix.

Hybrid nanocomposite can enhanced the electrical and thermal conductivity, optical and dielectric properties, and mechanical properties such as stiffness and strength (Ishii *et al.,* 2009). It is also reported that using hybrid nanocomposite enhance the toughness, ductility, corrosion resistance and competing specific strength (Alaneme *et al.,* 2015) compared to that of conventional composite.

### 2.1.2 Synthesis of nanocomposite

The common synthesis method of nanocomposite materials are bottom-up approach and top down approach. Bottom up synthesis approach use the phenomenon of assembly of atoms or particles. Bottom-up approach consists of chemical synthesis, chemical vapour deposition, thermal spray technique, inert gas condensation, rapid solidification and electro deposition. Meanwhile top-down approach refers to slicing or successive cutting of a bulk material to get nano sized particle. Top-down approach consists of processes mechanical alloying/milling, and spark erosion (Somani, 2006).

## 2.2 Ceramic Based Composite

Ceramic-based composite are usually classified into two material systems which are oxide-based and non-oxide-based. Oxide ceramics such as aluminium oxides or alumina ($Al_2O_3$) possessed high strength, hardness, corrosion resistance, and they are excellent electric insulators. However, the oxide ceramics suffer from relatively low fracture toughness and strength, significant degradation of mechanical properties at high temperatures and poor creep, fatigue and thermal shock resistances. Oxide-based CMCs consist of an oxide fiber and an oxide matrix such as $Al_2O_3$ whereas non-oxides can consist of carbon fibers with a carbon matrix (C/C), carbon fibers with a silicon carbide matrix (C/SiC), as well as silicon carbide fibers with a silicon carbide matrix (SiC/SiC) (Sun *et al.,* 1989). Non-oxide ceramic such as nitrides, carbides and borides undergo degradation of mechanical properties at high temperature due to slow crack growth which caused by the softening of grain boundaries (Indranil & Rajat, 2013; Niihara *et al.,* 1993).

Ceramic-based composite are widely used in many industries such as aerospace and electrical industries cutting tools, dental prostheses, thermal barrier coatings, as well as structural materials for the nuclear, energy, military, aerospace and building industries due to their excellent properties (Aigbodion *et al.,* 2010; Ding *et al.,* 2014; Low, 2014).

## 2.3 Alumina as Matrix in CMCs

Alumina ($Al_2O_3$) is an oxide of aluminum a group III element and very stable and robust material (Somani, 2006) (Figure 2.1). It has internal crystal structure where the oxygen ions are packed in a close-packed hexagonal arrangement. $Al_2O_3$ has several allotropic forms. $Al_2O_3$ has melting temperature of 2040°C (Auerkari, 1996).

It has high chemical and thermal stability, relatively good strength, chemical inertness, thermal and electrical insulation, high wear resistance and also has good mechanical properties (Meybodi *et al.,* 2013; Lach *et al.,* 2011).

Alpha phase $Al_2O_3$ is the strongest and the stiffest of the oxide ceramics. Its high hardness, excellent dielectric properties, refractoriness and good thermal properties make it the material of choice for a wide range of applications. Besides that, Alumina is the most widely used ceramic oxide because of its hardness, good corrosion resistance, availability in abundance and ease of processing (Guidara *et al.,* 2012; Auerkari, 1996). Mechanical properties of $Al_2O_3$ is shown in Table 2.1.

In addition, the strength of $Al_2O_3$ strongly depends on the types of acting forces or stresses as a result of low fracture toughness and the presence of imperfections. As similar to other ceramic based materials, alumina has higher degree of compressive strength, it is relatively brittle in nature under tensile and bending stresses. Additive can be added to enhance particular desirable material characteristics. $Al_2O_3$ is commonly used in many applications, such as cutting tools, electrical insulators, refractory materials and wear-resistance components.

However, there are drawbacks of $Al_2O_3$, due to its intrinsic stiff and brittle characteristics, $Al_2O_3$ exhibits in design limitations. Flexural strength of $Al_2O_3$, which is a mechanical parameter that is associated with brittleness the low, makes it unable to resist deformation under load over an extended period of time. $Al_2O_3$also has relatively low fracture toughness and thermal shock resistance which limits its more widely application, it is brittle and suffers from a drastic decrease in strength at high temperatures (Lee *et al.,* 2014; Meybodi *et al.,* 2013; Wang, 2016). Therefore, $Al_2O_3$ is reinforced either with metal, non-metal or hybrid materials.

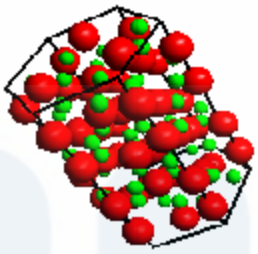

**Figure 2.1:** $Al_2O_3$ structure (Somani, 2006)

**Table 2.1:** Mechanical properties of $Al_2O_3$ (99 - 99.9 wt%) (Auerkari, 1996)

| **Mechanical Properties of $Al_2O_3$ (99 - 99.9 wt%)** | **Value** |
|---|---|
| Flexural strength | 550 MPa |
| Hardness | 15-16 GPa |
| Tensile Strength | 310 MPa |
| Compressive Strength | 3790 MPa |
| Fracture Toughness | 4.0 MPa |
| Modulus of Elasticity | 330-400 GPa |

## 2.4 Reinforcement materials in $Al_2O_3$-based nanocomposite

The addition of secondary ceramic reinforcement phase is one of the techniques to toughen $Al_2O_3$ ceramics (Huang *et al.*, 2014). There are a lot of material that can be reinforced with $Al_2O_3$ such as metal, ceramic or polymers. Whisker reinforcement can minimize the catastrophic brittle failure of $Al_2O_3$ via a range of toughening mechanisms, such as crack deflection, whisker pull out and bridging (Lee *et al.*, 2014). It also can be added by second phase or by the microstructure designs such as duplex or duplex-bimodal, heterogeneous and layer structures to improve its properties (Meybodi *et al.*, 2013). Furthermore, addition of a single nanoscale reinforcement to $Al_2O_3$ is reported to improve its physical and mechanical properties

(Mohammad *et al.,* 2016). On the other hand, fracture toughness and wear resistance of $Al_2O_3$ could also be enhanced with dispersion of nanometer sized particles.

Ceramics need to be reinforced because of their inherent brittleness and lack of reliability. Proper reinforcement of ceramics is aimed at increasing the resistance to crack propagation by introducing elements that arrest the cracks. For CMCs only those reinforcements that can withstand the high temperatures required by composite processing (above 1000°C) without significant damage can be used to reinforce ceramic.

### 2.4.1 Metal

Ceramic-based composite is well known for their brittleness. Addition of steel rods, wires, mesh will improve the brittleness and the fracture strength. Steel has the advantage of a similar thermal expansion coefficient, so there is reduced danger of cracking due to thermal stresses. In the other hand, electrical and thermal conductivity of ceramic matrix is increase with increasing metal content such as iron, chromium and stainless steel particle (Wildan *et al.,* 2002; Yongli, 2006). These composites are fabricated by hot-pressing fine ceramic and metal powder mixtures or by reducing and hot-pressing the matrix and metal oxide powders (Yongli, 2006).

### 2.4.2 Polymer

In CMC, only fiber components that can withstand the relatively high temperatures required for the production of ceramics, without damage. Other requirements to be met are long term high temperature stability, creep resistance, and

oxidation stability. Polymeric fiber materials cannot be used in CMC because of their degradation at temperatures below 500 ° C (Clauß, 2008).

### 2.4.3 Ceramic

Ceramic reinforcement that can be used in CMCs can be classified into oxide reinforcement and non-oxide reinforcement. Oxide reinforcement display high values of tensile strength and Young's modulus. As oxides, they are resistant to oxidation at high temperature. However, they creep under load at temperatures above 1100°C. When subjected to high temperatures over long times, they are sensitive to grain growth. Non oxide ceramic reinforcement exhibit superior tensile strength and creep resistance to oxide reinforcements (Lamon, 2011).

## 2.5 Hybrid reinforcement in $Al_2O_3$ -based nanocomposite

CMC can be reinforced with two or more reinforcement materials to become hybrid nanocomposite. The reinforcement can be in a group of metal, ceramic or polymers. In this study the focus is preparation of $Al_2O_3$-hybrid nanocomposite therefore, the discussion on using ceramic metal oxides ($TiO_2$) as reinforcement and graphite as filler will be elaborated.

### 2.5.1 Titania or titanium oxide

Titania ($TiO_2$) has three polymorphs which are of rutile, anatase and brookite (Somani, 2006) (Figure 2.2). $TiO_2$ has unique properties such as high chemical stability, defouling properties, high liquid flux and high photocatalytic activity, non-

environmental impact, and low cost, acting as a catalyst and being a semi-conductor (Habibpanah *et al.*, 2011).

$TiO_2$ is known as an effective additive to densify alumina below the normal densification temperature (Guidara *et al.*, 2012). The addition of $TiO_2$ to $Al_2O_3$ (ceramic matrix) considerably changed its sintering behaviour to manufacture dense ceramics. Furthermore, the fracture toughness and wear resistance of $Al_2O_3$ was improved with dispersion of $TiO_2$ (Bian *et al.*, 2012). However, excessive additions of $TiO_2$ may inhibit the densification of alumina because of the formation second phase of $Al_2O_{3-}$ $TiO_2$ at the grain boundary (Guidara *et al.*, 2012).

Although $TiO_2$ has been known as the most effective material for reinforcement, $TiO_2$ has relatively low surface area and the poor stability of the structure at high temperatures due to it instability of anatase structure (Habibpanah *et al.*, 2011; Sivakumar *et al.*,.2004) Therefore, much attention has been paid to applications of mixed oxides containing $TiO_2$

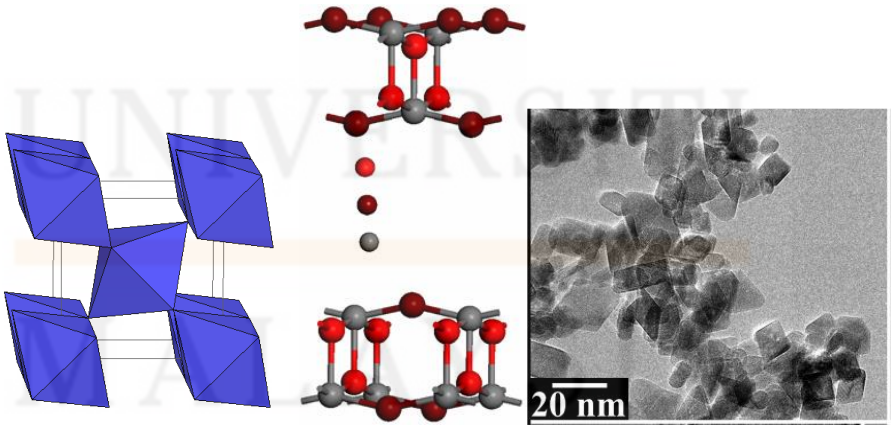


(a) (b) (c)

**Figure 2.2:** (a) Rutile structure in $TiO_2$ (b) Delaminated anatase unit cell with 8.7 Å interlayer spacing, (c) TEM image of anatase $TiO_2$ nanoparticles. (Mao *et al.*, 2006; Mogilevsky *et al.*,2008; Somani, 2006).

### 2.5.2 Graphite

Graphite is a polymorph of carbon and has crystal structure. Graphite formed as a layered of hexagonally arranged carbon atoms and the layers are packed closely by Van der Waals' force. As a consequence of this weak forces, interplanar cleavage is form, which gives rise to the lubricative properties of graphite. Graphite have high strength, good chemical stability at elevated temperature, high thermal conductivity, low coefficient of thermal expansion to thermal shock and high resistance to thermal shock, high mechanical and electrical properties, low density, easy processing and low cost (Gantayat *et al.*, 2015; Callister *et al.*, 2011)(Figure 2.3).

The lubricative properties of graphite serves as a solid lubricating layer between the composite and rubbing surface helping in reduction of composite wear without the need for traditional solid and liquid lubrication (Alaneme *et al.*, 2015). Addition of graphite results in decreasing of the strain at break and increasing the tensile strength of the composites. The thermal stability of composite is also enhanced with increasing the graphite percentage.

According to Girish *et al.*, 2011, the addition of graphite the friction coefficient of composites is decreased and the wear resistance increased by 170 to 340 times. Furthermore, according to Geric, 2010 when a few of volume percent of carbon (graphite) is added, a fracture toughness approximately 20% higher than that of the corresponding ceramic material containing no carbon additive, while the hardness and the flexural strength do not decrease much. On the other hand, due to its high thermal conductivity, graphite is commonly used as heating elements for electric furnace, as electrode for arc welding and high temperature refractories and insulators.

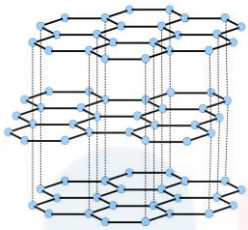

**Figure 2.3:** Structure of graphite (Gantayat *et al.*, 2015).

## 2.6 Processing method of CMC

Solid, liquid, or gas phase processing of ceramic matrix composites typically involve the infiltration of the matrix onto the reinforcement while processing. During processing of CMC, main objectives are attaining least porosity, uniform distribution of reinforcement and excellent bonding strength between fiber and matrix.

There are issues and challenges which limit the processing of CMC and therefore, the wide applications are also limited. Processing routes for CMC involve high temperatures and can only be employed with high temperature reinforcements, the high temperature properties of the reinforcement are also important during service and the difference in the coefficients of thermal expansion between the matrix and the reinforcement lead to thermal stresses after cooling from the processing temperatures.

There are many ways to fabricate CMC such as precise casting, forging and powder metallurgy, slurry infiltration/impregnation, polymer infiltration and pyrolysis, chemical vapour infiltration/impregnation, reaction bonding processes, directed oxidation, spark plasma sintering, sol gel method and in situ processing (Dehaghani *et al.*, 2014).

### 2.6.1 Powder metallurgy

Powder metallurgy (PM) involves of three routes which are milling, compaction and sintering. Milling is a process of using hard balls for mechanical impaction to fabricate powders from brittle materials. During milling, powder particles will undergo high-energy impacts by balls. The high energy impacts result in a high amount of defects such as vacancies, dislocations, grain boundaries in particles which in turn will change the nanometer crystallite size and phase transformations (Dehaghani *et al.,* 2014).

A jar mill consists of a cylindrical jar filled with balls and the material to be milled. As the jar rotates (Figure 2.4), the ball continuously collide with the material and crush it into powders. The energy required to reduce a powder to a smaller size depends on it relative changes in particle size. The time of milling depends on the particle size change, milling media size, and rotational velocity of the mill. Increasing milling time, the homogeneity of particle distribution is increased and improved and will be resulted in increasing the tensile strength (Sabzevari *et al.,* 2015).

Particle size will also decrease and matrix grain size will be deducted to sub micrometric level by increasing the milling time. Besides that, by increasing the milling time, coefficient of variation (COV) will be low (the lower the COV, the less clustered the distribution of particle). This will contribute to the increase in mechanical properties. Apart from a reduction in matrix grain size, it was determined that the texture of the studied materials also diminishes with increasing milling time.

Other than that, yield stress (YS) and ultimate tensile strength (UTS) clearly increase with increased milling time. The increase of YS and UTS is effected by dislocation strengthening mechanism between the matrix and reinforcement (Corrochano *et al.,* 2011; Mendoza *et al.,* 2015; Sabzevari *et al.,* 2015).

However, milling is not efficient for ductile materials since they do not easily fracture and instead they cold weld together. For brittle materials, milling is more efficient. During milling, the rotation of the jar is adjusted for maximum impact velocity which fast enough to carry the balls to the top of the jar before falling back. If the rotation is too slow, it will allow the balls to roll back down to the jar side and if it is too fast, it will create high centrifugal falls and keep the balls from falling.

The most optimal rotation speed for mill depends on the inverse square root of the mill diameter. Besides, the diameter of grinding balls should be approximate 30 times the diameter of the material for optimal milling. Furthermore, the volume of the balls should be half of the jar materials and the material should be 25% of the jar volume (German, 1997).

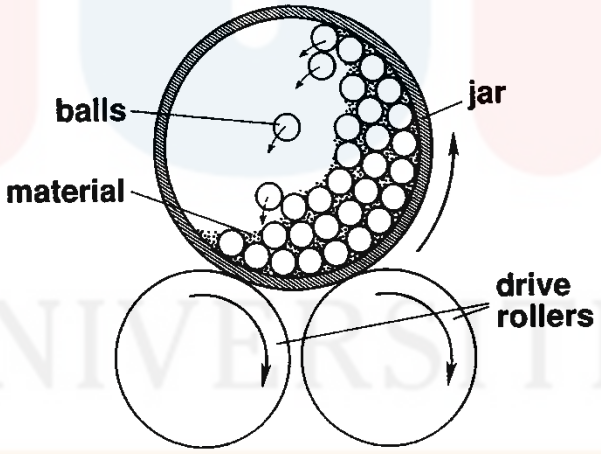


**Figure 2.4:** Ball milling (German, 1997)

Compaction is an important step in powder processing as it enables the forming of loose material powder into desired shape with sufficient strength. The powders are mixed with or without lubricant prior to compaction. The main purpose of compaction is to form powders compacts of desired shape with sufficient strength to withstand ejection from the tools and subsequent handling up to the completion of sintering

without breakage and damage. The degree of compaction use is maximized and the fraction of void spaces is minimized by using fine particles that mixed in appropriate proportion.

In ceramic materials, there is no plastic deformation of the particles during compaction. There are three basic powder-processing procedures which are uniaxial, isostatic (or hydrostatic) and hot pressing. For uniaxial pressing, the powder is compacted in a metal die by pressure that is applied in a single direction. The formed piece takes on the configuration of the die. Production rates are high and the process is inexpensive. The steps involved in one technique are illustrated in Figure 2.5. For isostatic pressing, the powder material is contained in a rubber envelope and the pressure is applied by a fluid isostically. More complicated shape can be form, however, there are more time consuming and expensive (Angelo *et al.,* 2012; Callister *et al.,* 2011). After powder compaction, the arrangement of particles can be shown as in Figure 2.6.

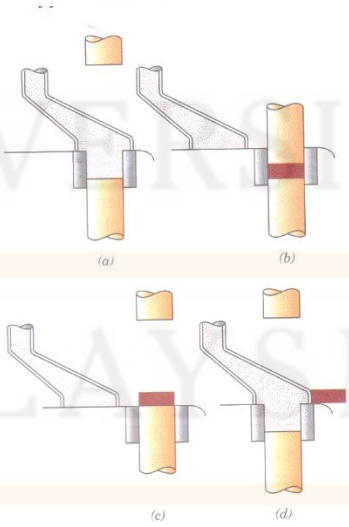


**Figure 2.5:** Steps in uniaxial powder pressing. (a) The die cavity is filled with powder, (b) the powder is compacted with pressure applied on the top, (c) the compacted powder is ejected, (d) the compacted powder is remove and the step is being repeat. (Callister *et al.,* 2011)

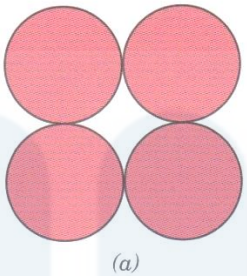


**Figure 2.6:** Powder particles after pressing. (Callister *et al.*, 2011)

Sintering is a process of consolidating either a loose arrangement of powder or a green compact of the desired composition under controlled condition of temperature and time. Sintering also known as the thermal treatment of a powder or compact at a temperature below the melting point of the material. During sintering, the compact is usually heated in protective atmosphere such as argon or hydrogen. Several changes take place during sintering like shrinkage, formation of solid solution and development of final microstructure.

During sintering, the process can be divided into three stages as shown in Figure 2.7. In the first stage, necks are formed at the contact points between the particles, which continue to grow. During the initial stage, rapid neck formation and neck growth takes place in the powder compact. During this stage the pores are interconnected and the pore shapes are irregular. In the second stage of sintering, with sufficient neck growth, the pore channels become more cylindrical.

Sufficient time in the sintering temperature the pore will become sphere and with continuous sintering, the pore channel pinch off and close. A network of pores and a skeleton of solid particles is formed. In this stage, migration of the grain boundaries between the original particles by grain growth takes place. The pores continue to form a more or less connected continuous phase throughout the compact. Shrinkage occur mainly in this stage. In the final stage, pore channel closure occur and

the pores become isolated and are no longer interconnected. The residual individual pores are located either at the grain boundaries or within the grain. In this stage, the porosity does not change and small pores remain even after long sintering time.

The densification proceed at a very slow rate. Sintering has a lot of types such as solid state sintering, liquid phase sintering, activated sintering, rate controlled sintering, microwave sintering, gas plasma sintering and spark plasma sintering (Angelo *et al.*, 2012; Callister *et al.*, 2011; German, 1997). A scanning electron micrograph of a sintered alumina material is shown in Figure 2.8 and scanning electron micrograph of a sintered $Al_2O_3$-$TiO_2$ material in Figure 2.9.

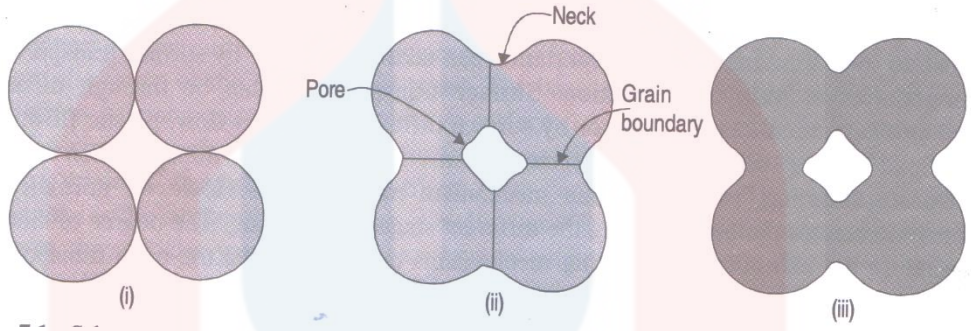


**Figure 2.7:** Microstructure of compacted powder during sintering. (i) Particles in contact, (ii) formation of necks, grain boundaries and pore, (iii) final sintered geometry (Angelo *et al.*, 2012).

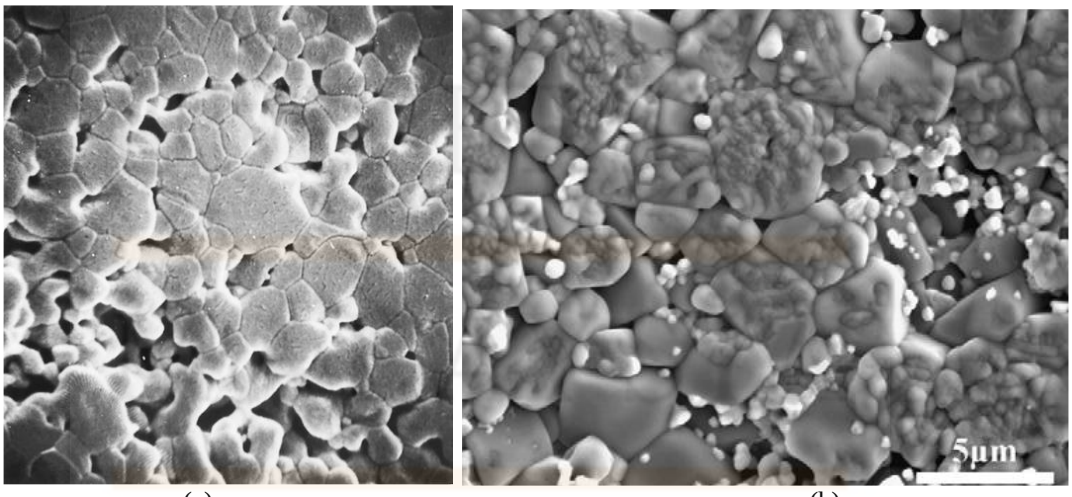


(a) (b)

**Figure 2.8:** (a) Scanning electron micrograph of an aluminium oxide powder compact sintered at 1700°C for 6 min. (b) Scanning electron micrograph of an alumina titania compact that was sintered at 1450°C (Callister *et al.*, 2011; Yang *et al.*, 2009)

There are a lot of advantages of PM compared to the other techniques which are the uniform distribution of reinforcing particles within the matrix and less degradation due to lower processing temperature. On the other hand, PM is a cost-effective production of simple and complex part and it also offers performance reliability in critical application. Moreover, PM alone can produce materials such as cemented carbide, refractory materials, oxide dispersion strengthened material, friction materials and porous materials.

Engineering applications of PM products consist of three groups which are, parts, which are impossible to manufacture by other methods, like porous bearings, filters, bimetallic copper lead alloy for use in hard bearing as well as hard and soft magnetic parts. Secondly, parts, which are difficult to make by other production as for example, parts made of tungsten, and molybdenum which cannot be made efficiently by any other process. Thirdly, components, where powder metallurgy is an effective alternative to parts made by casting and forging for example, small gears and connecting rods (Angelo *et al.,* 2012).

### 2.6.2 Chemical Vapour Infiltration (CVI)

CVI is a process where a porous preform is placed in a surrounding of a reactive gas mixture, which, if thermally activated, decomposes and yields a solid deposit that fills the pores inside the preform. The main advantages of this technique are the possibility to manufacture complex components at relatively low temperatures and to control and modify the microstructure of the matrix (Lazzeri, 2012). This technique allows the production of strong and tough composites and is ideal to produce composites with characteristics of resistance to corrosion, erosion, and wear.

Composites produced by CVI present excellent high temperature properties including high strength, modulus of elasticity, creep and corrosion resistance, resistance to shocks, fatigue and damage, chemical stability, and a greater fracture toughness. (Amirtha *et al.*, 2009). However, CVI densification are relatively costly and process times are lengthy, leading to high composite cost.

### 2.6.3 Melt Infiltration

Melt infiltration (MI) can be described as any technique of filling in pores by reaction with or deposition from a liquid. MI processing is rapid, requiring only a few hours to achieve nearly full density, and starting materials require only the availability of the respective metal or alloy (Zr metal for ZrC CMC), which is generally cost-effective.

However, the MI process does expose the fiber preforms to temperatures at or above the melting temperature of the respective alloy. The process requires the reinforcement fibers be protected from the melt during the MI process. In addition, not all of the metal reacts in situ during infiltration such that the matrix comprises a mix of the metal carbide and the unreacted metal (Stewart *et al.*,2014).

### 2.6.4 Polymer impregnation

The PIP process, consists in impregnating the polymeric precursor into a particulate bed, a porous solid or a fiber preform; heating to decompose and pyrolysis the polymer, and crystallizing following a firing schedule. The PIP process is simple to employ, and yields high purity of composite (Lee *et al.*, 2008). However, the fabrication time is relatively long and high production cost.

### 2.6.5 In situ processing

In situ method synthesize particulate reinforced phase within the matrix single step processing. Therefore, in-situ composites are multiphase materials where the reinforcing phase is synthesized within the matrix during composite fabrication while ex-situ in composites, the reinforcing phase is synthesized separately and then inserted into the matrix during a secondary process such as infiltration or powder processing. In-situ processes can create a variety of reinforcement morphologies, ranging from discontinuous to continuous, and the reinforcement may be either ductile or ceramic phases (Aikin, 1997). In situ method is more cost effective or material preparation compare to conventional processing (Zuhailawati *et al.*, 2009).

### 2.6.6 Sol gel method

Sol gel processing method provide an attractive and alternative routes to generate a homogenous and well distributed dispersion of reinforcement throughout ceramic matrix due to involve of the production of a sol containing ceramic particle, Where the reinforcement phase is mix and trapped in a gel network (Zapata *et al.*, 2012). Sol-gel is use because it offer several advantages like low temperature synthesis, ease in controlling composition variations, low cost and potential use in film processing (Somani, 2006).

According to Nenova *et al.*,2016 the sol gel method is a versatile method that enable development of entire new generation of composite materials. One of the methods of preparing composite sol is separately peptizing sol–gel (SP) procedure. In this way, the stable composite sols were prepared by physical mixing of the individual material sols (Habibpanah *et al.*, 2011). Sol-gel processing involves the use of a hydrolysis reaction to obtain a cross-linked network, which results in the formation of

a gel. The gel properties may be controlled by adjusting the pH level, water to metal ratio, and temperature (Kaplan *et al.*, 2006). Sivakumar *et al.*, 2004 reported that new sol–gel routes, involving no hydrolysis and resulting in gels with high degree of homogeneity is use for the preparation of binary oxides.

### 2.6.8 Slurry Infiltration/Impregnation

Slurry infiltration process is mainly used to fabricate ceramic matrix composites because the processing temperatures for these materials are lower than any other materials (Krishan, 2013). In this process, the matrix in the form of a liquid or slurry which infiltrates the fibre preform resulting in a composite. In other words, in this process, impregnation of the reinforcing phase takes place in a tank containing the matrix phase (liquid slurry). The slurry typically consists of matrix powder, liquid carrier (water or alcohol) and an organic binder. Various parameters such as particle size distribution, binder type and amount, powder content and carrier medium have a significant effect on composite part quality.

The matrix powder is the most important aspect of this process as the liquid carrier and the organic binder is removed during the process. The particle size of the matrix powder should be less than the fibre diameter as it results in reducing porosity as well as leads to thorough impregnation. Infiltration into the fibre preform can be improved by adding certain wetting agents in the slurry. After infiltration, the liquid carrier is allowed to evaporate. The resulting prepreg (a combination of fibre reinforcement and the slurry) can then be layed-up on a tool for consolidation. The organic binder must be burnt out before starting the consolidation process. This process is use widely because it is cost effective and easy to employ (Ohji *et al.*, 2010).

The slurry infiltration process involves two main stages. Stage one is the incorporation of the reinforcing phase into slurry of the consolidated matrix. The fibres are impregnated by passing them through the slurry tank. The impregnated fibres are then taken over by the take up drum. The prepreg thus formed is in the form of tapes which is cut into the desired size. Then, the different layers of tapes are stacked together and the binder is burnt out before the consolidation takes place. Stage two is matrix consolidation by hot pressing. After the burning of the binder from the stacked tapes, it is subjected to consolidation by hot pressing which results in the desired ceramic matrix composite. Slurry infiltration process results in fairly uniform distribution, low porosity and high strength. However, this process restricted to low melting or low softening point matrix materials (Krishan, 2013).

# CHAPTER 3

# MATERIALS AND METHOD

## 3.1 Introduction

This research involves of two stages which are preparation and characterization of the composite. The overall research experiment for this research is shown in Figure 3.1.

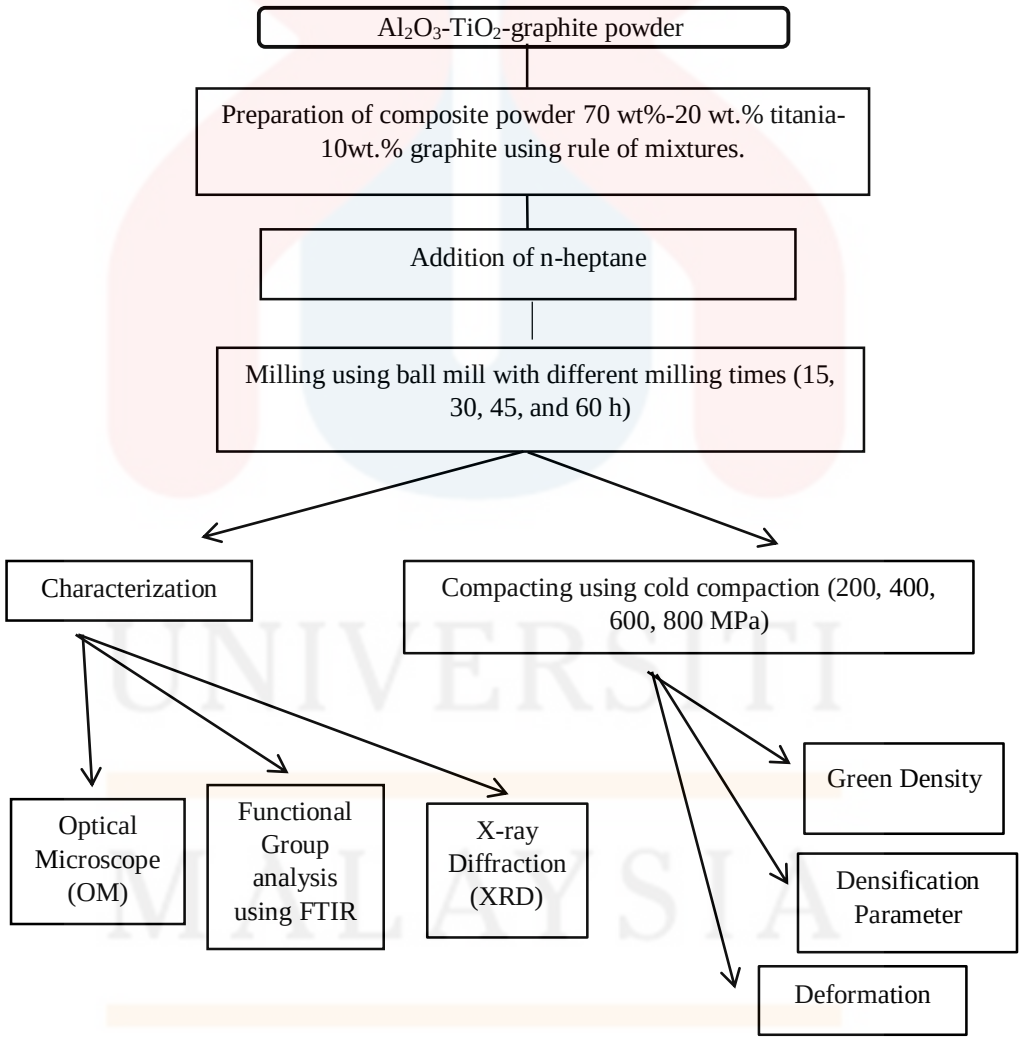


**Figure 3.1:** Overall research experiment in this research

### 3.2 Raw Materials

Materials that were used in this experiment are $Al_2O_3$ powder, $TiO_2$ powder and graphite powder.. $Al_2O_3$ (> 99.9% purity, average particle size > 20 µm), anatase $TiO_2$ (> 99.5% purity, average particle size >21 nm) and graphite (99.9% purity, average particle size > 20 µm) were used in study and were purchased from Sigma Aldrich.

### 3.3 Composite preparation

$Al_2O_3$–$TiO_2$-graphite nanocomposite were fabricated using powder metallurgy method. The composition of 70 wt%-20 wt.% titania-10 wt.% graphite mixture was used and were calculated using rule of mixture. The illustrated diagram of composite preparation is shown in Figure 3.2.

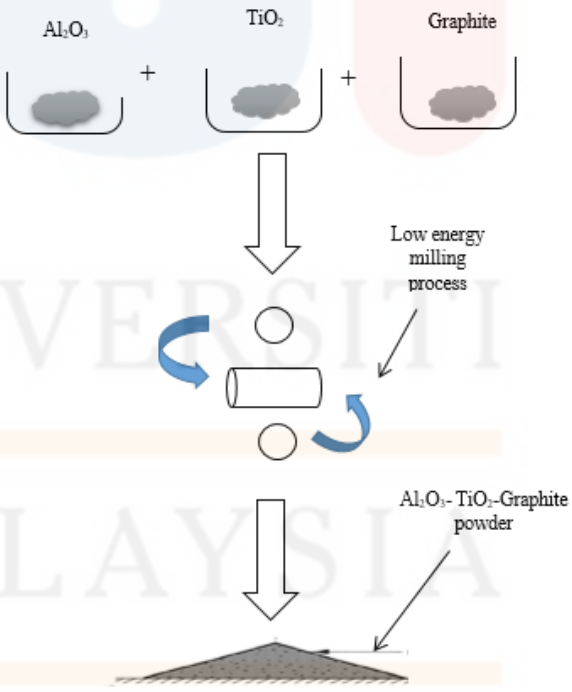


Figure 3.2: Illustrated diagram of milling process

### 3.3.1 Milling

Prior to milling, n-heptane was added to powder mixture with 2 wt% of total weight of the composite powder mixture. Then, the powder mixture were milled using low energy ball milling (Figure 3.3) with different milling times (15, 30, 45 and 60 h). During milling, alumina balls with diameter size 10 mm were used. The ratio of alumina balls to powder was 10:1 and milling speed used was 200 rpm.

Figure 3.3: Low energy ball milling machine

### 3.3.2 Cold compaction

Prior to compaction, the die was cleaned and coated with lubricant oil in order to decrease internal friction and increase powder compressibility during compaction. The composite powder mixture then compacted using uniaxial single action hydraulic press (Figure 3.4) in a stainless steel die at different pressures (200, 400, 600, 800 MPa). The stainless steel die has the diameter of 10 mm. The compaction process is shown in Figure 3.5.


Figure 3.4: Uniaxial single action hydraulic press

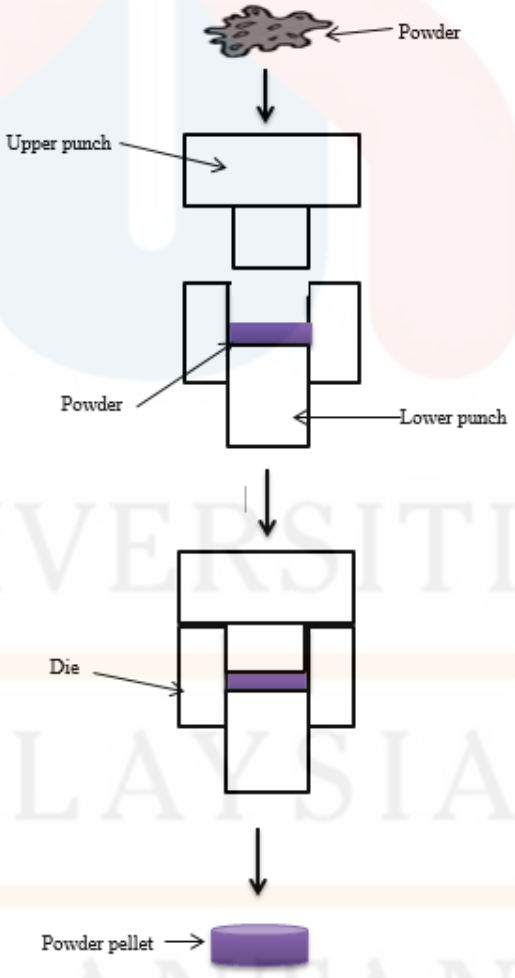


Figure 3.5: Compaction process of powder

### 3.4 Composite characterization

After the preparation of composite was done, they were characterized for phase analysis, microstructure and its density and densification.

#### 3.4.1 Phase analysis

The $Al_2O_3$-$TiO_2$-graphite nanocomposite were characterized for its phase identification using X-ray Diffraction (XRD) (Bruker D2 Phaser). The step size was fixed at 0.02° with the 2θ angle of 20° to 90°. Software DIFFRAC.EVA was used for phase identification to perform analysis on XRD pattern of the composite. The information from peak pattern were used to determine crystallize size and internal strain. Williamson-Hall (WH) method was used in this study to measure the crystallite size and internal strain. WH is the most common method used to evaluate the crystallite size and internal strain of milled composite powders. The assumption is that the whole line broadening, $B_o$ is a sum of the total broadening of size, lattice strain and instrument (Cullity & Stock, 2001):

$$B_o = B_i - B_{crys} + B_{strain} \quad \text{Eq.1}$$

Where $B_i$ broadening due to instrumental, $B_{cryst}$ broadening due to crystallite size and $B_{strain}$ broadening due to strain. Subtracting the instrumental effect, Eq. 2 (Cullity & Stock, 2001) becomes:

$$B_r = B_{crys} + B_{strain} \quad \text{Eq.2}$$

Where $B_r$ represent the overall broadening after eliminating the instrument broadening. Therefore, due to crystallite size and internal strain, WH method is given by (Williamson & Hall, 1953):

$$B_r \cos\theta = \frac{k\lambda}{D} + \eta \sin\theta \quad \text{Eq.3}$$

where η is internal strain $B_r$ is crystallite size, λ is the wavelength of the X-Ray used (1.5406 Å), θ is the Bragg angle, k is a constant and L can be obtained from observed FWHM by convoluting Gaussian profile with sample broadening. Only three $Al_20_3$ Bragg's peaks of (114), (213) and (216) reflections were considered for calculating $Al_20_3$ crystallite size and internal strain since they are the most highest and have the closest match from XRD database. The slope of plot of $B_r\cos\theta$ against sin θ either in positive or negative sides indicates the connection whether the sample in stress or stress-free state. Since the hkl (114), (213) and (216) reflections were derived from the same crystallite therefore, a straight line was drawn, according to the data points.

### 3.4.2 Functional Group Analysis using FTIR

In addition, Fourier transform infrared (FTIR) spectrometer was used to determine the adsorption of organic molecules in raw materials and nanocomposite. FTIR spectra was evaluated using Thermo Scientific TM iD7 with single-bounce attenuated total reflectance (ATR) technique. The FTIR spectra were recorded in the scanning range of 400–4,000 $cm^{-1}$ at 4 $cm^{-1}$ with 16 scans. The analysis of infrared spectra on the raw materials and nanocomposite were done using OMNIC spectra software.

### 3.4.3 Microstructure

The morphology of the composites were examined by optical microscopy (OM) using 20x magnification.

### 3.4.4 Density and densification parameter

After compaction, the dimension and mass of composite were measured. These information were calculated green density using general calculation of green density, GD as follows (Eq.4):

$$GD = \frac{m}{V} \qquad \text{Eq.4}$$

where *m* is mass and *V* is volume.

In order to study the compressibility of produced composite, densification parameter were calculated. Densification parameter will be determine using Eq. 5:

$$\text{Density} = \frac{GD - AD}{TD - AD} \qquad \text{Eq.5}$$

where AD is apparent density and TD is theoritical density.

# CHAPTER 4

# RESULTS AND DISCUSSION

## 4.1 Phase Identification of XRD

X-ray diffraction (XRD) was used to identify the structural properties of milled composite powders. Diffract.Eva software was used to find the matches pattern of $Al_2O_3$, $TiO_2$ and graphite powders. The information gathered from peak pattern also used to calculate crystallite size and internal strain.

### 4.1.1 Phase Identification

Figure 4.1 shows the XRD pattern for elemental powder and milled powder mixture for different milling time with 10 mm alumina ball. The elemental powders were observed to have crystalline structure. The analysis shows that the $Al_2O_3$ powders has three strong peaks at hkl (114), (213) and (216). However, $TiO_2$ has no strong peak because all of their peak are relatively small and broad. Graphite powder has only one strong peak at (111). The effect of milling time affects the broadening of each phase in the composite powder.

At 15 h of milling, the highest peak of $Al_2O_3$ and $TiO_2$ at 20.5° and 20.3° were almost overlapped, since their peak are very close to each other. Furthermore, $Al_2O_3$, $TiO_2$ and graphite phases were close match to the position of the elemental powders. Five $Al_2O_3$ peaks can be determined at 37.8°, 43.3°, 52.5°, 66.3° and 68.1° become broadened.

There were also a very little shift and broadening of the peaks as the milling time increased. This is due to low energy milling used and milled time of 15 h, 30 h,

45 h, 60 h are not enough and did not brought any new phase formation. As the milling time increase, graphite peak also drastically become shorter and finally at 60 h, graphite peak was diminished. Peak disappearance in XRD often used to represent the dissolution of second element into the matrix, forming solid solution with matrix or any other phase (Kellar, 2006).

Graphite peak diminished due to its faster diffusion into the $Al_2O_3$ matrix. At 60 h, a few of $TiO_2$ peaks also diminished due to small size and cause it to diffuse into $Al_2O_3$ matrix. Milling caused all $Al_2O_3$ peaks reduced and became wider because of the grain refining and internal stress accumulation induced by cold deformation and additional presence of tiny particles of the second phase which could introduce defects in the matrix (Inoue & Hirasawa, 2013).

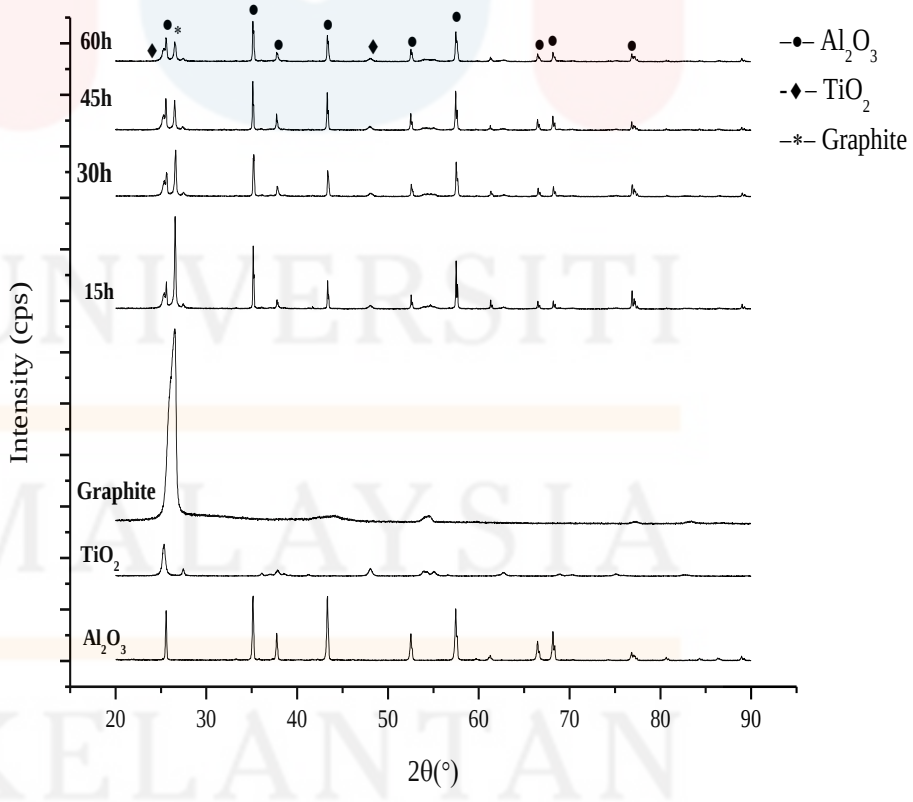


Figure 4.1: XRD pattern of elemental and milled powders.

### 4.1.2 Crystallite Size and internal strain

Crystallite size are usually taken as the cube root of the volume of a crystallite assumes that all crystallites have the same size and shape. For a distribution of sizes, the mean size can be defined as the mean value of the cube roots of the individual crystallite volumes and the cube root of the mean value of the volumes of the individual crystallites.

In this study, the crystallite size was determined from full width at half maximum (FWHM) and angle was extracted from obs.max in Diffarc.EVA software of hkl (114), (213) and (216) using Williamson Hall (WH) method. Figure 4.2 shows the plot of $B_r\cos\theta$ was plotted against the sin θ derived from WH method to determine the crystallite size and internal strain of the milled composite powder. $B_r\cos\theta$ was plotted against the sin θ and the strain is extracted from the slope and the crystalline size is extracted from the y-intercept of the fit. It can be seen that the slope and intercept has positive value indicate the reduction of crystallite size and increasing internal strain as the milling time increase.

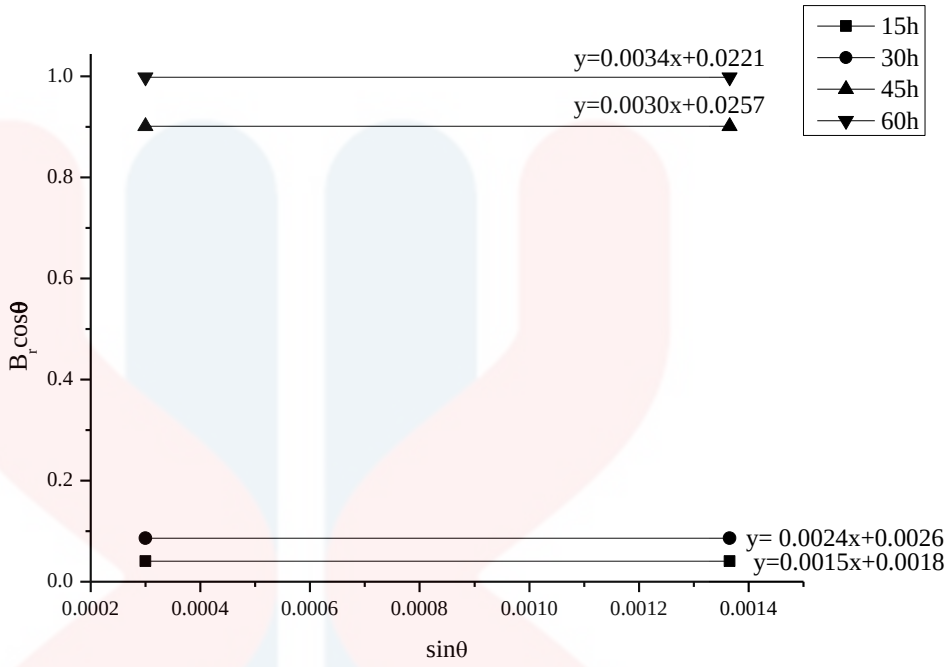


Fig. 4.2: Plot of $B_r\cos\theta$ against $\sin\theta$ for calculating crystallite size and internal strain in for the powder milled.

Figure 4.3 shows the effect of milling time to the crystallite size and internal strain of the powders. As the milling time was increased, a reduction tendency of the crystallite size was observed in all samples. Reduction of crystallite size was resulted by the interaction between the crystallites that tend to grow during the process (Beltrán *et al.,* 2015). The crystallite size of the composite decreased from 89.95 to 58.76 nm after 30 h of milling. After 60 h of milling, the crystallite size decrease to 39.152 nm. Decreasing crystallite size is due to the introduction of defects such as dislocations within grain during milling.

Furthermore, strain is defined as the deformation of an object divided by its ideal length, $\frac{\Delta d}{d}$. In crystals, there are two types of strain which are uniform strain and non-uniform strain. Uniform strain causes the unit cell to expand or contract in an isotropic.

It can be observed when milling time increased, the internal strain increased. At 15 h to 30 hours of milling, the internal strain did not increase rapidly while after 30 h the internal strain increase rapidly due to the stress produced during the collisions between the powders and the ball-mill. Other than that, the rapid increase of internal strain also indicates the strain hardening of the powders due to ball-milling (Ogawa & Masuda, 2015).

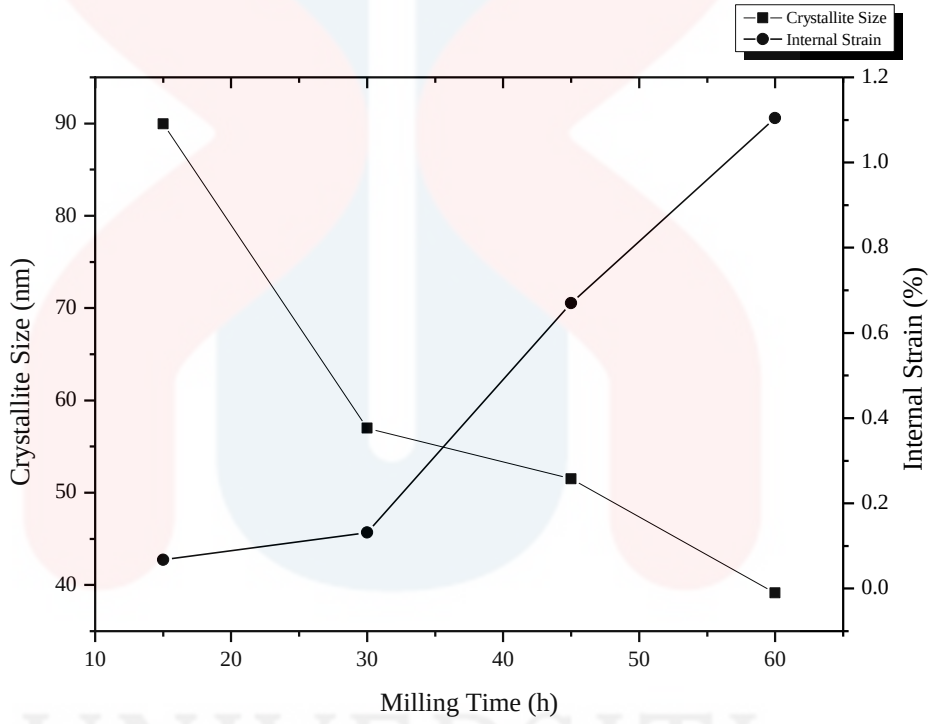


Figure 4.3: Crystallite size and internal strain of milled powder with different milling times.

**4.2 Microstructure of milled powder**

Microstructure of pure powder before mixing and milling at different milling times captured using optical microscope (OM) are shown in Figure 4.3. Starting powder of $Al_2O_3$ powder and graphite powder are slightly bigger than $TiO_2$ powder due to their powder size. $Al_2O_3$ powder and graphite powder has average size of 20 µm while $TiO_2$ powder has average size of 20 nm.

The particle distribution are uniformly distributed in all milling time with irregular shape but have different particle size. The influence of the milling process on the morphological evolution of matrix powders can be seen in these micrographs. It was found that the morphology of the matrix particles changed and the average particle size decreased slightly.

It can be seen that before milling process took place, graphite powders are bigger compare to after 60 h of milling. This is because, during the experiment, low energy milling was used to mill the powder. Low energy defines the condition of milling process that provides the break of agglomerated particles in the agglomerate position only.

However, if the time of milling is long enough, the milling process is able to allow the radical break up of particles. The break up position can be in both agglomerate and main body of crystal positions. As a result, dispersed slurry contains multisized particles as can be seen after 60 h of milling (Tahara *et al.*, 2014).

The size of powder particles at 60 h are smaller and well distributed compared to 15 h. This is because increasing milling time induced the reduction of particle size and matrix grain size are deducted to sub micrometric level. At 60 h, the homogeneity of particle distribution is also enhanced.

Besides, prolonging the milling time, lower the coefficient of variation (COV) and produced less clustered particle distribution (Mendoza, 2015). Apart from a reduction in matrix grain size, it was determined that the shape of the studied materials also diminishes with increasing milling time.

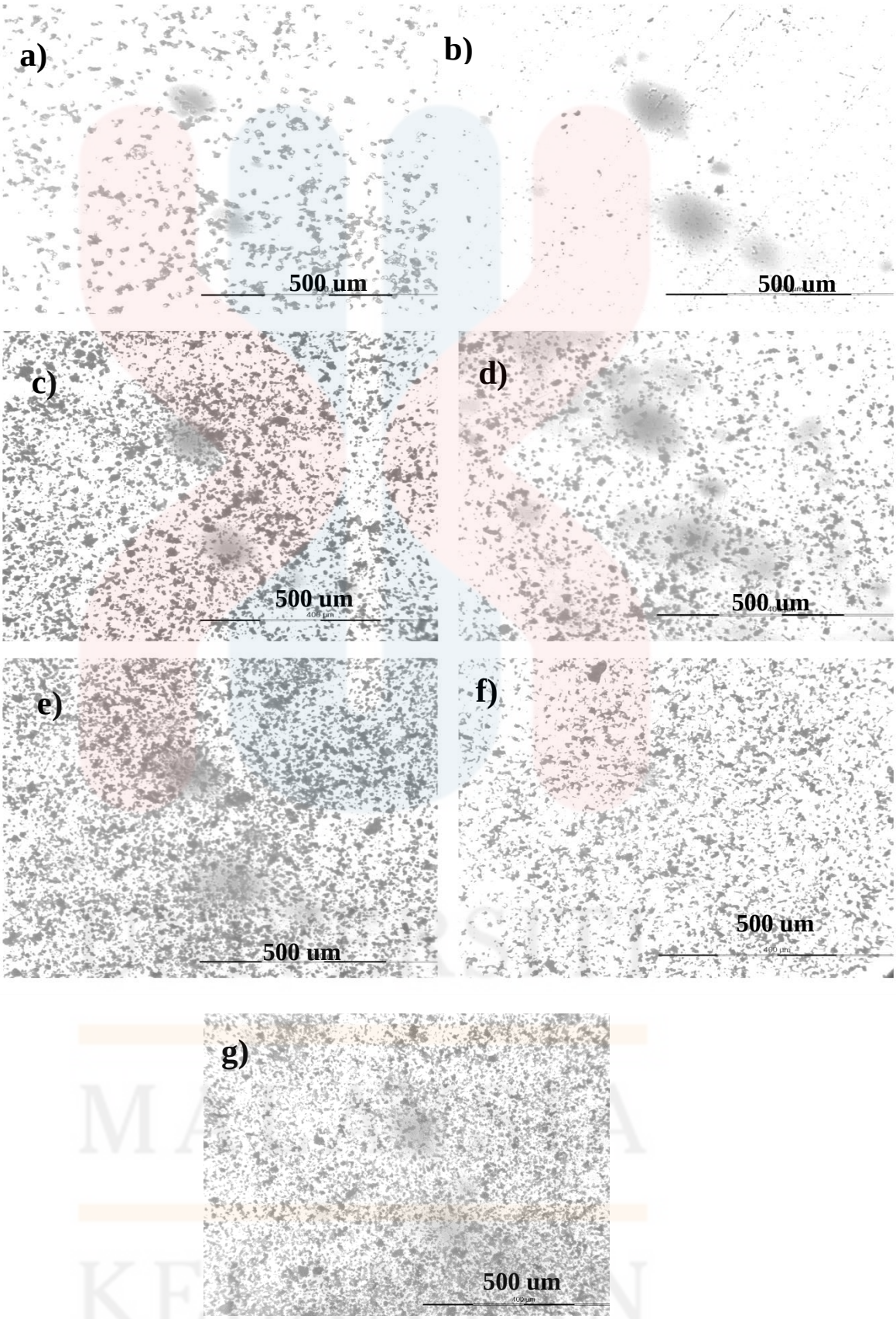


Figure 4.4 a) Optical microscope image of $Al_2O_3$ powder b) $TiO_2$ powder c) graphite powder. Optical microscope image of $Al_2O_3$- $TiO_2$ -graphite powder with d) 15 h e) 30 h f) 45 h g) 60 h

### 4.3 Properties of $Al_2O_3$-$TiO_2$ – graphite nanocomposite

After the milling process, the composite powder were compacted using uniaxial single action hydraulic press using stainless steel die at different pressures (200, 400, 600, 800 MPa). Then the density and densification parameter of the composite were calculated.

#### 4.3.1 Green Density

The compaction of powdered materials is carried out primarily to increase the density of the material. The ultimate goal of the over-all process is to obtain minimum porosity.

Figure 4.5 shows green density of the composite powder at different compaction pressure. Higher the compaction pressure higher the green density. This is because when pressure applied equally on all sides of a material, called isostatic pressure, it caused a reduction in volume, consequently leading to an increase in density. Volume reduction only results from the application of isostatic pressure. Applying pressure uniaxially or biaxially causing the material to expand in directions that it is not constrained.

Higher pressure also caused the porosity to decrease. The smaller particles such as $TiO_2$ and graphite powder filled the void of within the $Al_2O_3$ matrix. Furthermore, when the powder were compacted using axial loading in a die or hydrostatic pressure it may effectively reduce the porosity of most powders (Heckel, 1960). Hence, it affects the density of the compacted powder and caused the density to increase with increasing compaction pressure.

Besides, according to Suresh *et al.*, 2015 high loading generates shear and is extremely beneficial for plastic deformation of powder particles, which results in high green densities. This prove that with increase of pressure the green density will also increase.

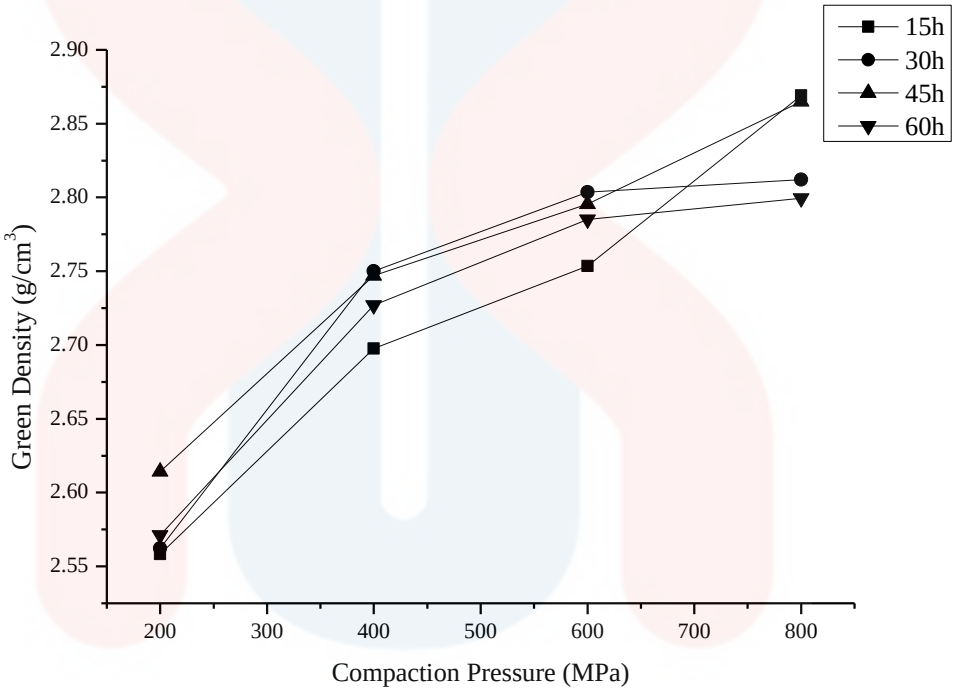


Figure 4.5: Green density of $Al_2O_3$- $TiO_2$ -graphite powder with different milling time against different compaction pressure

### 4.3.2 Densification Parameter

Densification parameter of the composite are plotted against different compaction pressure shown in Figure 4.6. During compaction, loose powder is shaped in a die using a mechanical or hydraulic press giving rise to densification. The mechanisms of densification depend on the material and structural characteristics of powder particles. It was found that densification parameter is proportionated to the

applied compaction pressures. This can be explained by the particle size distribution and the porosity of the nanocomposite with different milling time. The densification parameter follows similar trend as green density because green density affect the densification parameter (Padmavathi & Upadhyaya, 2010).

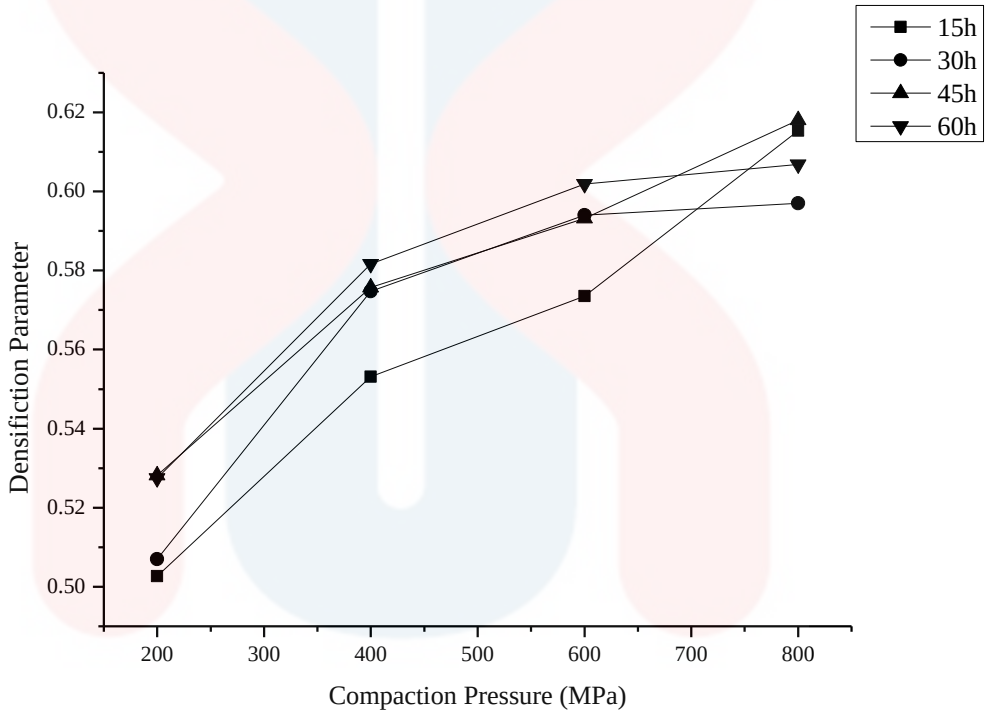


Figure 4.6: Densification parameter of $Al_2O_3$- $TiO_2$ -graphite powder with different milling time against different compaction pressure

During compaction, the process is characterized by three distinct phases namely re-arrangement of powder particles, inter-particle sliding and plastic deformation of powder particles. With increasing densification, the powder particles are plastically deformed and caused the graphite to fill the gaps between iron particles resulting in higher densities due to the lubricative properties of graphite. In order to co-relate between the applied compaction pressure and relative density or porosity for

all the compacted powders, the equation proposed by Panelli and Ambrozio Filho (Panelli & Filho, 2001) can be used:

$$\ln\left[\frac{1}{1-D}\right] = AP^{\frac{1}{2}} + B \qquad \text{Eq. 6}$$

Where D is relative density of the compacted material and P is the compaction pressure.

$\ln\left[\frac{1}{1-D}\right]$ is plotted against $AP^{\frac{1}{2}}$ in Figure 4.7. A is the slope represent the plastic deformation while the intercept represents the densification parameter. It can also be seen in Figure 4.6 that with higher milling time, the plastic deformation is also enhanced. This is probably due to the higher density was obtained in higher milling time since it has more fine particles with broad distribution compared to that of lower milling time composite powder.

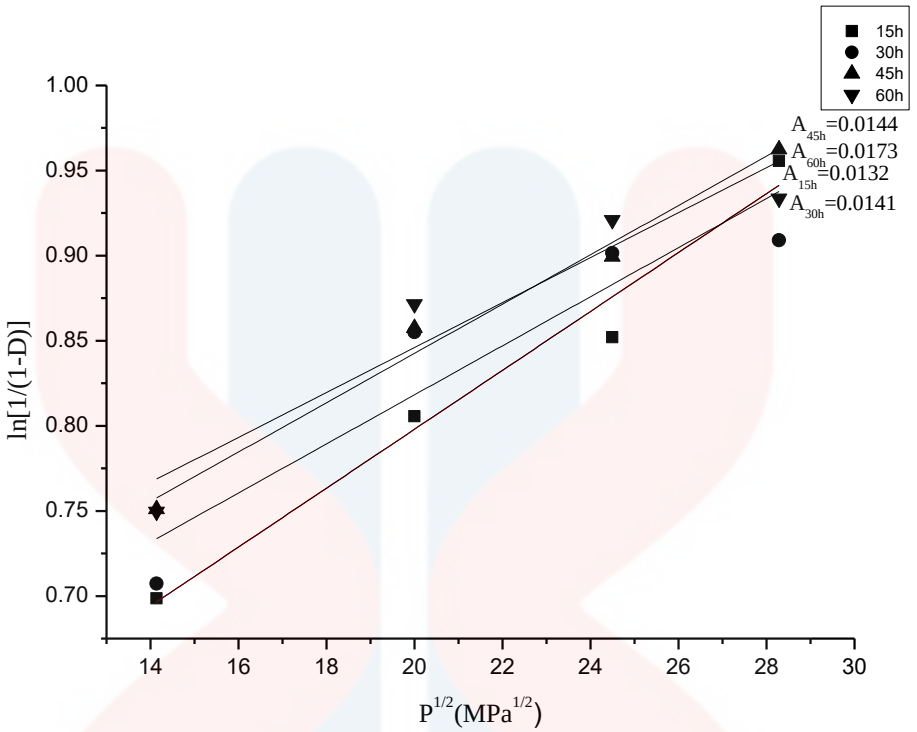


Figure 4.7: Plot of experiment data for green compact using the equation proposed by Panelli and Ambrozio Filho (1998)

### 4.4 Functional Group Analysis (FTIR)

In order to evaluate the functional groups of the synthesized $Al_2O_3$-$TiO_2$-graphite powders, FTIR analysis was done and can be presented in Figure 4.7. $Al_2O_3$-$TiO_2$-graphite milled powders were compared to $Al_2O_3$-$TiO_2$ milled powder to see if there were changes or formation of bonding in composite powder.

FTIR analysis in Figures 4.7 and 4.8 show several variations in adsorption peaks of the $Al_2O_3$, $TiO_2$, graphite powders and $Al_2O_3$-$TiO_2$-graphite milled powders at different time. Saturated peak of $TiO_2$ (Figure 4.7) at below than 700 $cm^{-1}$ was assigned to Ti–O and Ti–O–Ti bonding of $TiO_2$. The small peak at 3215 and 3747 $cm^{-1}$ is attributed to stretching of –OH groups in the composite powder. $Al_2O_3$ powder however, has insignificant functional group bonding found in its spectrum despite of

having a few small peaks. Graphite powder has three significant peak at 1990.78, 2112.92 and 1734.98 $cm^{-1}$. Despite of having relatively broad and weaker spectrum, there are one inorganic nitrates bond found at 1400 $cm^{-1}$.

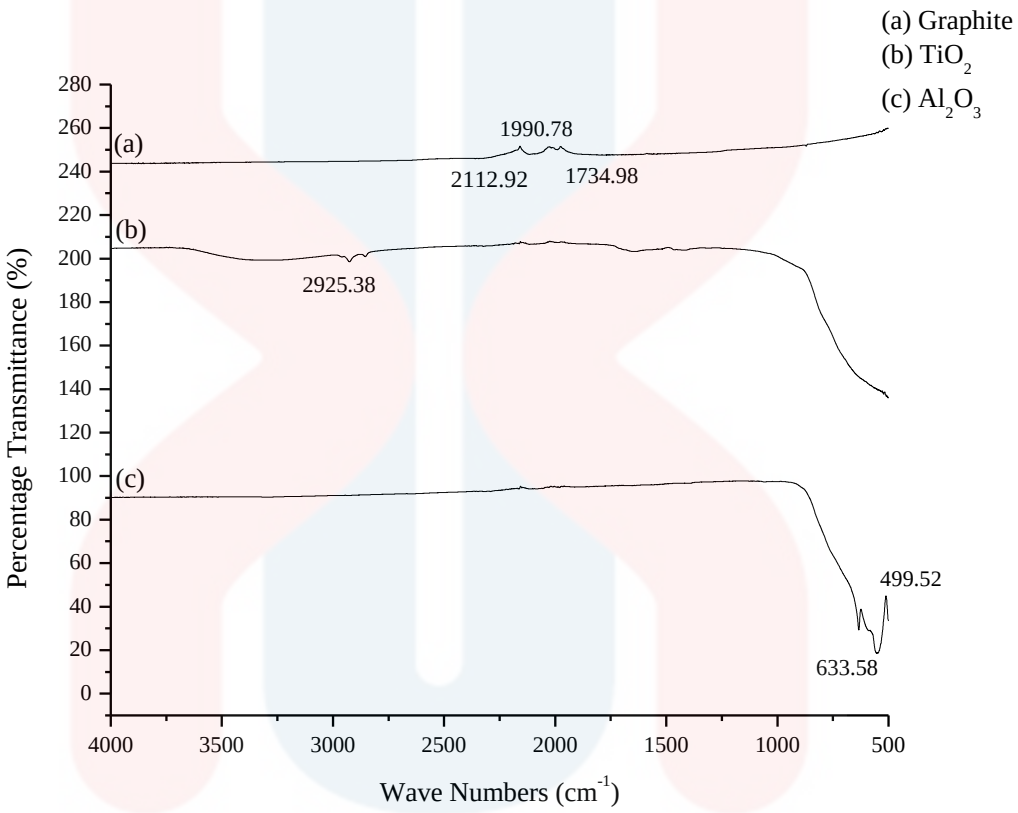


Figure 4.8: FTIR spectra of starting powders a) graphite, b) $Al_2O_3$ and c) $TiO_2$.

Figure 4.9 compares the FTIR spectrum of milled $Al_2O_3$-$TiO_2$-graphite powder and $Al_2O_3$-$TiO_2$ powder at different milling time. With the presence of graphite, $Al_2O_3$-$TiO_2$-graphite spectrum are broader and flat compare to $Al_2O_3$-$TiO_2$ milled powders. $Al_2O_3$-$TiO_2$ milled powders has aliphatic hydrocarbon bonds at three of its peak. However, $Al_2O_3$-$TiO_2$-graphite powders shows no bond in all milling time even though hat they have several strong peaks.

Bonding that are originally from pure $TiO_2$ and graphite might have been diminished after they were mixed with $Al_2O_3$ powders. Used of low energy milling also one of the reason that there was no new bond form between the reinforcement phase and the matrix. This is due to the fact that there was not enough energy to enhance the formation of new phase or new bond. If the milling time is prolonged, they might be a new bond formation between the reinforcement phase and the matrix phase.

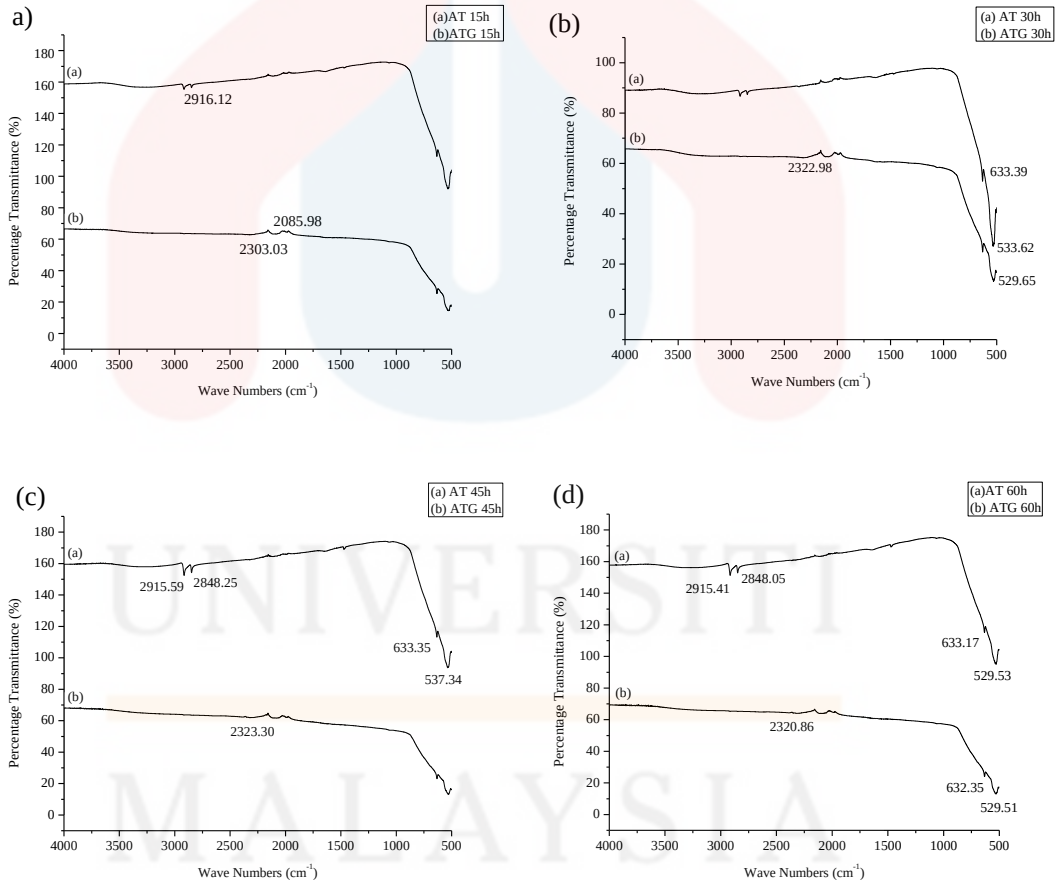


Figure 4.9: FTIR spectra of a) ATG 15h and AT 15 h b) ATG 30 h and AT 30 h c) ATG 45 h and AT 45 h and d) ATG 60 h and AT 60 h

# CHAPTER 5

# CONCLUSION

## 5.1 Conclusions

In this study, the effort to prepare nanostructured in situ $Al_2O_3$- $TiO_2$ -graphite hybrid nanocomposite by Powder Metallurgy has been successful. Preparing the milled powder was carried out by milling elemental $Al_2O_3$, $TiO_2$ and graphite powders. Bulk composite was prepared by compaction. The conclusions were drawn from variations of milling period and compaction pressure:

1. Variations of milling time affect the microstructure and structural properties of $Al_2O_3$- $TiO_2$ –graphite hybrid nanocomposite.
2. Increasing milling time caused the changes of $Al_2O_3$-$TiO_2$–graphite composite powder internal structure and morphology.
3. Increasing milling time decreased the crystallite size of $Al_2O_3$ and increased the internal strain of $Al_2O_3$-$TiO_2$–graphite composite powder.
4. Higher milling time produced composite with fine powders and less agglomeration.
5. Higher compaction pressure increase the green density, densification parameter and deformation of the $Al_2O_3$-$TiO_2$–graphite hybrid nanocomposite.

## 5.2 Recommendation

It has been recognized that tailoring the PM parameters has changed the nature of microstructure and properties of composite. Using low energy milling did not really shows a big phase changing and no new phase was produced. For the future, milling with higher speed can be used and longer milling time can be applied.

Other than that, the used of optical microscope did not allow the fine particle to be seen. In the future, the use of scanning electron microscope (SEM) is highly recommended.

Furthermore, it is suggested that the nanocomposite will be sintered so that the microstructural and structural properties can easily observed.

Besides, it is also suggested that in future, there will be mechanical testing to study the impact of milling time and compaction pressure on the strength of the nanocomposite.

## References


Aigbodion, V. S., Agunsoye, J. O., Kalu, V., Asuke, F., Ola, S., Metallurgical, N., & Centre, D. (2010). Microstructure and Mechanical Properties of Ceramic Composites, *9*(6), 527–538.

Aikin, R. m. (1997). The Mechanical Properties of In-Situ Composites. *The Mineral, Metals &material*, *49*(8), 35–39.

Alaneme, K. K., & Sanusi, K. O. (2015). Microstructural characteristics, mechanical and wear behaviour of aluminium matrix hybrid composites reinforced with alumina, rice husk ash and graphite. *Engineering Science and Technology, an International Journal*, 1–7.

Angelo, P. c., & subramaniam, p. (2012). *Powder Metallurgy*. *PHI Learning Private Limited*.

Auerkari, P. (1996). Mechanical and physical properties of engineering alumina ceramics. *Technical Research Centre of Finland*, *1792*, 26.

Banga, H., Singh, V. K., & Choudhary, S. K. (2015). Fabrication and Study of Mechanical Properties of Bamboo Fibre Reinforced Bio-Composites, *6*(1), 84–99.

Bhattacharya, S. N., Kamal, M. R., & Gupta, R. K. (2007). Preparation and Synthesis. *Polymeric Nanocomposites*, *18*, 5–33.

Bian, H., Yang, Y., Wang, Y., & Tian, W. (2012). Preparation of nanostructured alumina – titania composite powders by spray drying , heat treatment and plasma treatment. *Powder Technology*, *219*, 257–263.

Casati, R., & Vedani, M. (2014). Metal Matrix Composites Reinforced by Nano-Particles—A Review. *Metals*, *4*(1), 65–83.

Callister, G. rethwisch, david. (2011). *Materials Science and Engineering*. john wiley & sons.

Çelik, Y., Çelik, A., Flahaut, E., & Suvaci, E. (2016). Anisotropic mechanical and functional properties of graphene-based alumina matrix nanocomposites. *Journal of the European Ceramic Society*, *36*(8), 2075–2086.

Clauß, B. (2008). Fibers for Ceramic Matrix Composites. *Ceramic Matrix Composites*, 1–20.

Corrochano, J., & Lieblich, M. (2011). The effect of ball milling on the microstructure of powder metallurgy aluminium matrix composites reinforced with MoSi2 intermetallic particles. *Composites Part A: Applied Science and Manufacturing*, *42*(9), 1093–1099.

Cullity, B. ., & Stock, S. . (2001). *Elements of X-Ray Diffraction*. Pearson Education Limited.

Ding, P., Su, S., Song, N., Tang, S., & Shi, L. (2014). Highly thermal conductive composites with polyamide-6 covalently-grafted graphene by an in situ polymerization and thermal reduction process. *Research Center of Nanoscience and Nanotechnology, Shanghai University, Shanghai 200444, PR China*, *Volume 66*, 576–584.

Donald, I. W., & McMillan, P. W. (1976). Ceramic-matrix composites. *Journal of Materials Science*, *11*(5), 949–972.

G. Amirthan , A. Udayakumar , V. V. Bhanu Prasad, and M. B. (2009). Properties of Si/SiC ceramic composite subjected to chemical vapour infiltration. *Ceramic Industry*, *35*, 2601–2607.

Gantayat, S., Prusty, G., Rout, D. R., & Swain, S. K. (2015). Expanded graphite as a filler for epoxy matrix composites to improve their thermal , mechanical and electrical properties. *New Carbon Materials*, *30*(5), 432–437.

Geric, K. (2010). Ceramics Tool Materials With Alumina Matrix. *Machine Design*, *3*, 367–372.

German, randal m. (1997). *Powder Metallurgy Science*. Metal Powder Industries Federation.

Girish, B. M., Prakash, K. R., Satish, B. M., Jain, P. K., & Devi, K. (2011). Need for optimization of graphite particle reinforcement in ZA-27 alloy composites for tribological applications. *Materials Science & Engineering A*, *530*, 382–388.

Guidara, A., Chaari, K., & Bouaziz, J. (2012). Effect of Titania Additive on Structural and Mechanical Properties of Alumina-Fluorapatite Composites. *Journal of Materials Science and Technology*, *28*(12), 1130–1136.

Habibpanah, A. A., Pourhashem, S., & Sarpoolaky, H. (2011a). Preparation and characterization of photocatalytic titania – alumina composite membranes by sol – gel methods, *31*, 2867–2875.

Habibpanah, A. A., Pourhashem, S., & Sarpoolaky, H. (2011b). Preparation and characterization of photocatalytic titania-alumina composite membranes by sol-gel methods. *Journal of the European Ceramic Society*, *31*(15), 2867–2875.

Heckel, R. W. (1960). Density-Pressure Relationships in Powder Compaction.

Huang, J., & Nayak, P. K. (2014). Strengthening alumina ceramic matrix nanocomposites using spark plasma sintering. *Advances in ceramic matrix composites*. Woodhead Publishing Limited.

Indranil & Rajat, (2013). *Ceramic Nanocomposite*. (1st ed.). Woodhead.

Ishii, T., & Shigehara, K. (2009). Hybrid Nanocomposites for Nanotechnology. *Business*, 2–24.

Kaplan, W. ., & A, A. (2006). Processing and microstructural control of metal-reinforced ceramic matrix nanocomposites. *Processing*.

Kellar, J. j. (2006). *Functional Fillers And Nanoscale Minerals*. ( John. J Kellar, Ed.). Society for Mining, Metallurgy, and Exploration, Inc. Retrieved from

Krishan K., C. (2013). *Composite Materials: Science and Engineering*. technology & engineering. Retrieved from

Lach, R., Haberko, K., Bućko, M. M., Szumera, M., & Grabowski, G. (2011). Ceramic matrix composites in the alumina/5-30vol.% YAG system. *Journal of the European Ceramic Society*, *31*(10), 1889–1895.

Lamon, J. (2011). Ceramic reinforcements for composites. *Composite Reinforcements for Optimum Performance*, 51–85.

Lazzeri, A. (2012). *CVI Processing of Ceramic Matrix Composites*. *Ceramics and Composites Processing Methods*.

Lee, D. Y., & Yoon, D. H. (2014). Properties of alumina matrix composites reinforced with SiC whisker and carbon nanotubes. *Ceramics International*, *40*(9 Part A), 14375–14383.

Lee, S. G., Fourcade, J., Latta, R., & Solomon, A. A. (2008). Polymer impregnation and pyrolysis process development for improving thermal conductivity of SiCp/SiC-PIP matrix fabrication. *Fusion Engineering and Design*, *83*(5–6), 713–719.

Low, I. M. (2014). *1 - Advances in ceramic matrix composites: an introduction*. *Advances in Ceramic Matrix Composites*. Woodhead Publishing Limited.

Makisima, A. (2004). possibility of hybrid material. *Ceramic Japan*, *39*, 90–91.

Mao, Y., & Wong, S. S. (2006). Size- and shape-dependent transformation of nanosized titanate into analogous anatase titania nanostructures. *Journal of the American Chemical Society*, *128*(25), 8217–8226.

Mendoza-Duarte, J. M., Estrada-Guel, I., Carreno-Gallardo, C., Martinez-Sa, & Nchez, R. (2015). Study of Al composites prepared by high-energy ball milling; Effect of processing conditions. *Journal of Alloys and Compounds*, 1–6.

Meybodi, S. M., Barzegar Bafrooei, H., Ebadzadeh, T., & Tazike, M. (2013). Microstructure and mechanical properties of $Al_2O_3$–20wt%$Al_2TiO_5$ composite prepared from alumina and titania nanopowders. *Ceramics International*, *39*(2), 977–982.

Mogilevsky, G., Chen, Q., Kleinhammes, A., & Wu, Y. (2008). The structure of multilayered titania nanotubes based on delaminated anatase. *Chemical Physics Letters*, *460*(4–6), 517–520.

Mohammad, K., & Saheb, N. (2016). Molecular level mixing: An approach for synthesis of homogenous hybrid ceramic nanocomposite powders. *Powder Technology*, *291*, 121–130.

Nenova, Z., Kozhukharov, S., Nenov, T., Nedev, N., & Machkova, M. (2016). Combined influence of titania and silica precursors on the properties of thin film humidity sensing elements prepared via a sol-gel method. *Sensors and Actuators, B: Chemical*, *224*, 143–152.

Niihara, K., Nakahira, A., & Sekino, T. (1993). New Nanocomposite Structural Ceramics. *Mat. Res. Soc. Symp. Proc.*, *286*, 405–412.

Ogawa, F., & Masuda, C. (2015). Microstructure evolution during fabrication and microstructure-property relationships in vapour-grown carbon nanofibre-reinforced aluminium matrix composites fabricated via powder metallurgy. *Composites Part A: Applied Science and Manufacturing*, *71*, 84–94.

Ohji, T., Jeong, Y.-K., Choa, Y.-H., & Niihara, K. (1998). Strengthening and Toughening Mechanisms of Ceramic Nanocomposites. *Journal of the American Ceramic Society*, *60*(6), 1453–1460.

Ohji, T., & Singh, M. (2010). *Advanced Processing and Manufacturing Technologies for Structural and Multifunctional Materials IV: Ceramic Engineering and Science Proceedings, Volume 31, Issue 8*. john wiley & sons.

Padmavathi, C., & Upadhyaya, A. (2010). Densification, microstructure and properties of supersolidus liquid phase sintered 6711Al-SiC metal matrix composites. *Science of Sintering*, *42*(3), 363–382.

Panelli, R., & Filho, F. A. (2001). A study of a new phenomenological compacting equation.

Pournaderi, S., Mahdavi, S., & Akhlaghi, F. (2012). Fabrication of $Al/Al_2O_3$ composites by in-situ powder metallurgy (IPM). *Powder Technology*, *229*, 276–

Prabu, M., Ramadoss, G., Senthilkumar, C., Magibalan, S., & Senthilkumar, P. (2016). Electric Discharge Machining of Al-TIB2 Composites With And Without Graphite Powder Suspended Dielectric, *11*(2), 1242–1244.

Sabzevari, M., Abdolkarim, S., & Moloodi, A. (2015a). Physical and mechanical properties of porous copper nanocomposite produced by powder metallurgy. *Advanced Powder Technology*, 5–11.

Santos-Beltrán, A., Goytia-Reyes, R., Morales-Rodriguez, H., Gallegos-Orozco, V., Santos-Beltrán, M., Baldenebro-Lopez, F., & Martínez-Sánchez, R. (2015). Characterization of $Al–Al_4C_3$ nanocomposites produced by mechanical milling. *Materials Characterization*, *106*, 368–374.

Sivakumar, S., Sibu, C. P., Mukundan, P., Pillai, P. K., & Warrier, K. G. K. (2004). Nanoporous titania – alumina mixed oxides — an alkoxide free sol – gel

synthesis, *58*, 2664–2669.

Somani, V. (2006). *Alumina-Aluminum Titanate-Titania Nanocomposite : Synthesis , Sintering Studies , Assesment of Bioactivity*.

Sternitzke, M. (1997). Structural ceramic nanocomposites. *Journal of the European Ceramic Society*, *17*, 1061–1082.

Stewart, T., Williams, B., & Brockmeyer, J. (2014). Melt-Infiltrated Refractory Ceramic Matrix Composites. *Ceramic Industry*.

Suresh, K. R., Mahendran, S., Krupashankara, M. S., & Avinash, L. (2015). Influence of Powder Composition & Morphology on Green Density for Powder Metallurgy Processes. *International Journal of Innovative Research in Science*, *4*(1), 18629–18634.

Taghian Dehaghani, M., Ahmadian, M., & Fathi, M. (2014). Effect of ball milling on the physical and mechanical properties of the nanostructured Co-Cr-Mo powders. *Advanced Powder Technology*, *25*(6), 1793–1799.

Tahara, T., Imajyo, Y., Nandiyanto, A. B. D., Ogi, T., Iwaki, T., & Okuyama, K. (2014). Low-energy bead-milling dispersions of rod-type titania nanoparticles and their optical properties. *Advanced Powder Technology*, *25*(5), 1492–1499.

Vijayaraghavan, G. (2007). Synthesis and Characterization of Carbon anotube Supported anoparticles for Catalysis. *Lib.Utexas.Edu*.

Wagner, H. D., & Roman, I. (n.d.). Hybrid effects in the bending stiffness of graphite / glass- reinforced composites, *17*, 1359–1363.

Wang, L. (2016). Reinforcing and Toughening Alumina / Titania Ceramic Composites with Nano-Dopants from Nanostructured Composite Powders, (May 2009).

Wildan, M., Edress, H, & Hendry, A. (2002). Ceramic matrix composites of zirconia reinforced with metal particles. *Materials Chemistry and Physics*, *volume 75*, 276–283.

Williamson, G, & Hall, W. . (1953). X-ray line broadening from filed aluminium and wolfram. *Metallurgy*, *1*(1), 22–31.

Yamada, H. Sasabe, Y. O. and Y. S. (1989). Concepts of Hybrid Materials, Hybrid Materials –Concept and Case Studies.

Yongli, L. (2006). *Nanophase ceramic composites*. (I. M. Low, Ed.). Woodhead Publishing Limited.

Yoon, S. Do, Byun, H. S., & Yun, Y. H. (2015). Characterization and photocatalytic properties of ceramics $TiO_2$ nanocomposites. *Ceramics International*, 1–6.

Zapata-Solvas, E., Gómez-García, D., & Domínguez-Rodríguez, A. (2012). Towards physical properties tailoring of carbon nanotubes-reinforced ceramic matrix composites. *Journal of the European Ceramic Society*, *32*(12), 3001–3020.

Zuhailawati, H., & Mahani, Y. (2009). Effects of milling time on hardness and electrical conductivity of in situ Cu-NbC composite produced by mechanical alloying. *Journal of Alloys and Compounds*, *476*(1–2), 142–146.

## APPENDIX

### Weight of $Al_2O_3$-$TiO_2$-graphite composite

a) 15 h

| Pressure (MPa) | Width (mm) | | Weight (g) | | Average width | Average weight |
|---|---|---|---|---|---|---|
| | sample 1 | sample 2 | sample 1 | sample 2 | | |
| 200 | 5.21 | 5.38 | 1.039 | 1.089 | 5.295 | 1.064 |
| 400 | 5.18 | 5.1 | 1.09 | 1.088 | 5.14 | 1.089 |
| 600 | 5.06 | 4.88 | 1.076 | 1.074 | 4.97 | 1.075 |
| 800 | 4.78 | 4.84 | 1.079 | 1.089 | 4.81 | 1.084 |

b) 30 h

| Pressure (MPa) | Width (mm) | | Weight (g) | | Average width | Average weight |
|---|---|---|---|---|---|---|
| | sample 1 | sample 2 | sample 1 | sample 2 | | |
| 200 | 5.62 | 5.31 | 1.129 | 1.071 | 5.465 | 1.1 |
| 400 | 5.2 | 4.98 | 1.119 | 1.08 | 5.09 | 1.0995 |
| 600 | 4.92 | 4.87 | 1.082 | 1.074 | 4.895 | 1.078 |
| 800 | 4.89 | 4.84 | 1.074 | 1.075 | 4.865 | 1.0745 |

c) 45 h

| Pressure (MPa) | Width (mm) | | Weight (g) | | Average width | Average weight |
|---|---|---|---|---|---|---|
| | sample 1 | sample 2 | sample 1 | sample 2 | | |
| 200 | 5.3 | 5.23 | 1.091 | 1.071 | 5.265 | 1.081 |
| 400 | 4.98 | 5.02 | 1.081 | 1.077 | 5 | 1.079 |
| 600 | 4.91 | 4.93 | 1.077 | 1.084 | 4.92 | 1.0805 |
| 800 | 4.75 | 4.88 | 1.065 | 1.102 | 4.815 | 1.0835 |

d) 60 h

| Pressure (MPa) | Width (mm) | | Weight (g) | | Average width | Average weight |
|---|---|---|---|---|---|---|
| | sample 1 | sample 2 | sample 1 | sample 2 | | |
| 200 | 5.46 | 5.19 | 1.08 | 1.071 | 5.325 | 1.0755 |
| 400 | 4.97 | 5.15 | 1.088 | 1.08 | 5.06 | 1.084 |
| 600 | 4.91 | 4.94 | 1.08 | 1.074 | 4.925 | 1.077 |
| 800 | 4.86 | 4.9 | 1.071 | 1.075 | 4.88 | 1.073 |

## Green Density

a) 15 h

| Pressure (Mpa) | mass (g) | volume (cm) | Green density |
|---|---|---|---|
| 200 | 1.064 | 0.4159 | 2.5583 |
| 400 | 1.089 | 0.4037 | 2.6975 |
| 600 | 1.075 | 0.3904 | 2.7536 |
| 800 | 1.084 | 0.3778 | 2.8692 |

b) 30 h

| Pressure (Mpa) | mass (g) | volume (cm) | Green density |
|---|---|---|---|
| 200 | 1.1 | 0.4293 | 2.5623 |
| 400 | 1.0995 | 0.3998 | 2.7501 |
| 600 | 1.078 | 0.3845 | 2.8036 |
| 800 | 1.0745 | 0.3821 | 2.8121 |

c) 45 h

| Pressure (Mpa) | mass (g) | volume (cm) | Green density |
|---|---|---|---|
| 200 | 1.081 | 0.4135 | 2.6143 |
| 400 | 1.079 | 0.3928 | 2.7469 |
| 600 | 1.0805 | 0.3865 | 2.7956 |
| 800 | 1.0835 | 0.3782 | 2.8649 |

d) 60 h

| Pressure (Mpa) | mass (g) | volume (cm) | Green density |
|---|---|---|---|
| 200 | 1.0755 | 0.4183 | 2.5711 |
| 400 | 1.084 | 0.3975 | 2.7270 |
| 600 | 1.077 | 0.3867 | 2.7851 |
| 800 | 1.073 | 0.3833 | 2.7994 |

## Apparent density

| Milling time (h) | Mass (m) | Volume (v) | Apparent Density (AD) |
|---|---|---|---|
| 15 | 5.893 | 5.029 | 1.1718 |
| 30 | 5.812 | 5.029 | 1.1557 |
| 45 | 5.74 | 5.029 | 1.1414 |
| 60 | 5.302 | 5.029 | 1.0543 |

**Densification parameter**

15 h

| Pressure (MPa) | Densitification Parameter |
|---|---|
| 200 | 0.5027 |
| 400 | 0.5532 |
| 600 | 0.5735 |
| 800 | 0.6154 |

30 h

| Pressure (MPa) | Densitification Parameter |
|---|---|
| 200 | 0.5070 |
| 400 | 0.5747 |
| 600 | 0.5940 |
| 800 | 0.5970 |

45 h

| Pressure (MPa) | Densitification Parameter |
|---|---|
| 200 | 0.5282 |
| 400 | 0.5758 |
| 600 | 0.5932 |
| 800 | 0.6180 |

60 h

| Pressure (MPa) | Densitification Parameter |
|---|---|
| 200 | 0.5275 |
| 400 | 0.5817 |
| 600 | 0.6019 |
| 800 | 0.6068 |